# Syntheses, structures and properties of group 12 element (Zn, Cd, Hg) coordination polymers with a mixed-functional phosphonate-biphenyl-carboxylate linker†

Christian Heering,[a] Biju Francis,‡[a] Bahareh Nateghi,[a] Gamall Makhloufi,[a] Steffen Lüdeke[b] and Christoph Janiak*[a]

The new phosphonate-carboxylate ligand from 4-phosphono-biphenyl-4′-carboxylic acid ($H_2O_3P-(C_6H_4)_2-CO_2H$, $H_3BPPA$) is based on the rigid biphenyl system and is studied toward the coordination behavior of group 12 elements zinc, cadmium and mercury. The crystalline products from hydrothermal syntheses highlight the versatile and different coordination modes with the (partially) deprotonated $H_3BPPA$ ligand to give coordination polymeric 3D-$[Zn_5(\mu_3\text{-}OH)_4(\mu_4\text{-}O_3P-(C_6H_4)_2-CO_2\text{-}\mu_2)_2]_n$ (5), 2D-$[Zn(\mu_6\text{-}O_3P-(C_6H_4)_2-CO_2H)]_n$ (6), 3D-$[Cd_3(\mu_5\text{-}O_3P-(C_6H_4)_2-CO_2\text{-}\mu_2)(\mu_6\text{-}O_3P-(C_6H_4)_2-CO_2\text{-}\mu_3)]_n$ (7) and 2D-$[Hg(\mu_3\text{-}HO_3P-(C_6H_4)_2-CO_2H)]_n$ (8). The cobalt complex, 2D-$[Co(\mu_4\text{-}O_3P-(C_6H_4)_2-CO_2H)]_n$ (9) is isostructural to 6. Through additional classic strong carbonyl O–H⋯O hydrogen bonding the dimensionality of the 2D coordination networks increases to 3D supramolecular frameworks. The carboxy-phosphonate ligand shows five different coordination modes which can be described as $\mu_4\text{-}O_3P-CO_2\text{-}\mu_2$ (5), $\mu_6\text{-}O_3P-$ (6), $\mu_5\text{-}O_3P-CO_2\text{-}\mu_2$, $\mu_5\text{-}O_3P-CO_2\text{-}\mu_3$ (7), and $\mu_3\text{-}O_3P-$ (8), that is, the ligand bridges altogether between 3 to 8 metal atoms with the phosphonate group alone connecting already 3 to 6 metal atoms. Layers of metal–oxygen polyhedra are interconnected via the biphenyl linker, which either coordinates metal atoms with both donor groups or the –COOH end forms tail-to-tail hydrogen bonds to create 3D or 2D coordination networks, respectively. In the flat {$MO_x$} layers in 6 and 7 the Zn and Cd metal nodes represent a honeycomb and an mcm net, respectively. The coordination polyhedra of the Cd atoms in compound 7 were analyzed towards a trigonal-prismatic coordination environment. The complexes are hydrolytically very stable due to their hydrothermal preparation from aqueous solution at 180–200 ºC. The compounds could be stored in water or air for months without apparent decomposition. Compounds 5 and 7, where the ligand is fully deprotonated, start to decompose at ~400 ºC. The fluorescence emission spectrum of the ligand, 4, shows an intense peak at 365 nm ($\lambda_{ex}$ = 316 nm). The fluorescence emission of the metal complexes 5, 7 and 9 is shifted towards larger wavelengths with values of 417 nm, 415 nm and 410 nm, respectively ($\lambda_{ex}$ = 354 nm for 5, $\lambda_{ex}$ = 350 nm for 7, $\lambda_{ex}$ = 400 nm for 8, $\lambda_{ex}$ = 360 nm for 9). In addition, the crystal structures of the $H_3BPPA$ ligand precursors 4-iodo-4′-biphenylcarboxylic acid methyl ester, and 4-diethylphosphono-4′-biphenylcarboxylic acid methyl ester are described here for the first time.

[a] Institut für Anorganische Chemie und Strukturchemie, Universität Düsseldorf, Universitätsstr. 1, 40225 Düsseldorf, Germany. E-mail: janiak@hhu.de
[b] Institut für Pharmazeutische Wissenschaften, Universität Freiburg, Albertstr. 25, 79104 Freiburg, Germany
† Electronic supplementary information (ESI) available: NMR data for 1–4, IR data for 1–9, additional structure graphics, bond lengths and angles, TGA and PXRD data for 4–9, photos of crystals (5, 7, 8, 9), geometrical calculations for 5–8, and CD spectra of 5. CCDC 1465329–1465334. For ESI and crystallographic data in CIF or other electronic format see DOI: 10.1039/c6ce00587j
‡ Permanent address: CSIR-Network of Inst. for Solar Energy, National Institute for Interdisciplinary Science & Technology (NIIST), Thiruvananthapuram-695 019, India.

## Introduction

Metal–organic frameworks, MOFs, and coordination polymers became a rapidly growing research area in recent years, because of possible applications,[1,2] for example in catalysis,[3] sensing by fluorescence changes,[4,5] gas storage[6,7] and separation.[8,9] However, the water or moisture stability of such networks is often low.[10]

One approach to increase hydrothermal stability is the use of three- or four-valent, highly charged metal ions such as $Cr^{3+}$, $Al^{3+}$, $Fe^{3+}$, $Ti^{4+}$ or $Zr^{4+}$ in MIL-MOF compounds[11–14] (MIL = Materials of Institute Lavoisier) or UiO-MOFs[15] (UiO

University of Oslo).[16–18] Carboxylate linkers were also replaced by azolates with improved stability of analogous or isoreticular compounds.[19,20] Yet, the focus has seldom been set on very strongly coordinating (organo)phosphonate groups,[21,22] which could significantly raise the stability of such metal–ligand coordination compounds.
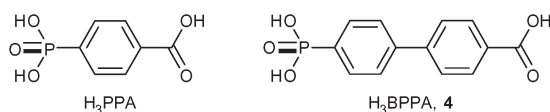
Organophosphonic acids, which have a $pK_{a1}$ of 2.0 for the first and a $pK_{a2}$ of 6.59 for the second proton, are more acidic ligands than pyrazoles ($pK_a$ = 2.49). Organophosphonates generate strong metal–ligand coordinative bonds in thermodynamically stable complexes with high stability constants. Metal organophosphonate compounds are organic–inorganic hybrid materials,[23] can be porous networks,[24–27] and as such be placed in between zeolite-like[28,29] and metal–organic framework materials.[30] Metal organophosphonates are stable in water or aqueous environment[31] and can be reversibly hydrated and dehydrated.[27,32–36] The use of metal phosphonates in catalysis, luminescence,[37] ion or proton exchange or conductivity[38,39] and in separation is discussed and investigated.[40] Cobalt and iron organophosphonates exhibit magnetic properties.[41–48]

Organophosphonates can contain additional functional groups such as carboxylate, hydroxyl or amino in the organo-moiety which presents a tunable functionality with a wide variety of structural motifs and properties.[49]

The controlled growth of crystalline metal–organophosphonate complexes is not a straightforward procedure.[28] This is probably due to the strong metal–ligand bond, which is formed with little reversibility to correct for crystal defects. Therefore, we started to investigate carboxyl-phosphonate ligands,[50] which can be seen as intermediates between pure carboxylates and pure phosphonates, and share synergies of both ligand classes. Metal complexes with mixed-functional 4-phosphono-benzoic acid (H$_3$PPA) (Scheme 1 and S1 in ESI†) with barium,[51] cobalt,[52] copper,[52] europium,[53] lead,[54] lithium,[55] silver,[56] strontium,[57] thorium,[58] titanium,[59] uranium[58] and zinc[55,60,61] are known. Carboxy-phosphonates can form porous or 3D metal–ligand networks.[62–64] Weng et al. described a 3D zinc carboxy-phosphonate, ZnPC-2, as a material for $CO_2$ adsorption.[65] As in MOFs, di- or tri-substituted rigid phosphonato-aryl-carboxylate linkers are a rational choice for rigid networks.

Here we present the synthesis of the new mixed-functional linker 4-phosphono-4′-biphenylcarboxylic acid, H$_3$BPPA (4) (Schemes 1 and 2) and four crystal structures of coordination networks with the group 12 metal ions zinc, cadmium and mercury.

The concept of a mixed-functional rigid linker with carboxylate and phosphonate coordinating groups was used to

obtain hydrothermally stable coordination networks. Up to now, no carboxy-phosphonate complexes with mercury have been known or published to the best of our knowledge.

## Results and discussion

### Linker synthesis

The linker H$_3$BPPA has been synthesized for the first time here (Scheme 2), following a known procedure by Merkushev et al. to synthesize 4′-iodo-biphenyl-4-carboxylic acid (1) through the iodination of 4-biphenyl carboxylic acid.[66] Compound 1 was transformed into the carboxy methyl ester 2, followed by the nickel(II) catalyzed conversion to a phosphonate ester (3), which after hydrolysis gave H$_3$BPPA (4).

Crystals of the 4-iodo-4′-biphenylcarboxylic acid methyl ester (2) were obtained by slow evaporation of a chloroform solution. The crystal structure of compound 2 shows a nearly in-plane conformation of both aryl rings and the carboxy methyl ester group (Fig. 1a). The dihedral angle between both aryl rings is 1.4(3)° and between the plane of the –COOMe
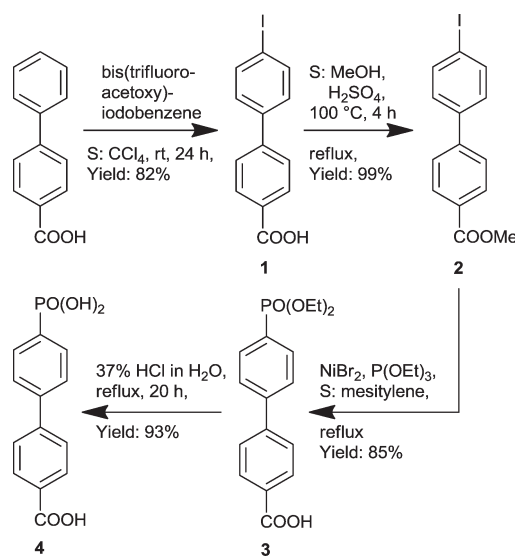
**Scheme 2** Reaction sequence for the synthesis of H$_3$BPPA (4) from 4-biphenyl carboxylic acid.
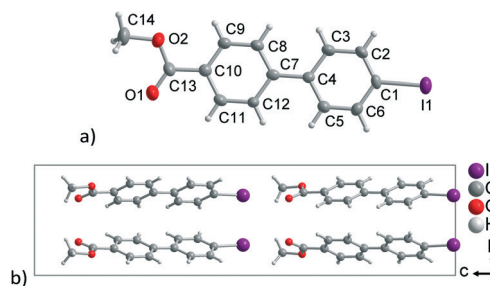
**Fig. 1** (a) Asymmetric unit (50% thermal ellipsoids) and (b) projection of the unit cell packing of **2**. Selected distances (Å) and angles (°): C1–I1 2.082(9), C13–O1 1.202(13), C13–O2 1.303(12), O1–C13–C10 123.4(9), O1–C13–O2 123.6(10).

**Scheme 1** 4-Phosphono-benzoic acid (H$_3$PPA) and 4-phosphono-4′-biphenylcarboxylic acid (H$_3$BPPA, **4**).

group and its aryl ring it is 8.1(6)°. In 4-biphenyl carboxylic acid the dihedral angle between the –COOH group and the aryl ring is 29.05° and the dihedral angle between both aryl rings is 2.89°.[67] This implies a better π-conjugation in the 4-iodo-derivative **2**. Compound **2** crystallizes in the non-centrosymmetric orthorhombic space group $Pca2_1$. The non-centrosymmetric packing (Flack parameter 0.080(17))[68] originates from the identical orientation of the iodo or carboxyl groups, respectively, along the crystallographic $c$ axis at an angle of ±21.7(8)° (Fig. 1b).

Crystals of 4-diethylphosphono-4′-biphenylcarboxylic acid methyl ester (**3**) were derived from mesitylene solution. In the crystal structure of compound **3** (Fig. 2) the carboxy methyl ester and aryl ring form a dihedral angle of 13.7(2)°, the two aryl rings a dihedral angle of 35.8(2)°.

The thermal stability of the phosphono-carboxylic acid **4** (mp > 350 °C, decomp. > 400 °C, see TGA in Fig. S18 in ESI†) is higher than that of biphenyl-4,4′-dicarboxylic acid, which has a melting point of 310 °C.[69]

## Metal compound syntheses and structures

Due to poor solubility of the phosphono-carboxylic acid in most common solvents, the reactions between ligand and metal salts were carried out under hydrothermal conditions at high temperatures (up to 180 °C) in water. All five metal complexes **5–9** share the common coordination motif of layers of metal ions, bridged by either carboxylate and phosphonate or the phosphonate group only (Scheme 3).

The zinc compound $[Zn_5(\mu_3\text{-}OH)_4(\mu_4\text{-}O_3P\text{-}(C_6H_4)_2\text{-}CO_2\text{-}\mu_2)_2]$ (**5**) was obtained from a 3 : 2 molar ratio of $Zn(OAc)_2$ and $H_3BPPA$ in water in the presence of oxalic acid. Oxalic acid was added as a buffer to give stable pH values. There was little effect on the yield or product composition when the reactant stoichiometry was adjusted to the ratio found in the X-ray structure in subsequent repeated reactions.
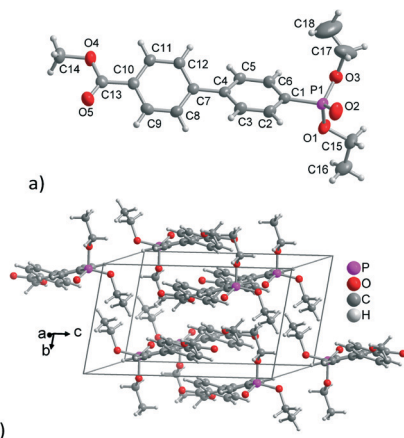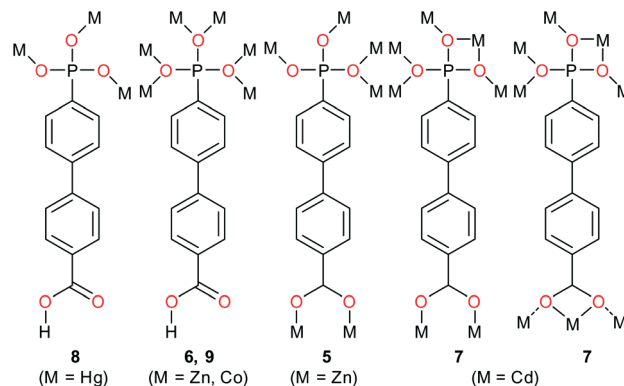
**Fig. 2** (a) Asymmetric unit (50% thermal ellipsoids) and (b) crystal packing in **3**. Selected distances (Å) and angles (°): P1–O1 1.560(2), P1–O2 1.462(2), P1–O3 1.567(2), C13–O5 1.195(3), C13–O4 1.341(3), O1–P1–O2 116.11(13), O2–P1–O3 113.98(13), O1–P1–O3 102.44(13).

**Scheme 3** Coordination modes of the BPPA ligand in the structures of **5–9**. The metal atom (M) can be Zn, Cd, Hg or Co.

The structure of **5** consists of Zn(II) ions that are coordinated by hydroxide ions and either carboxylate (–COO⁻) or phosphonate groups (–PO₃²⁻). The asymmetric unit contains three crystallographically different zinc atoms (one of them, Zn3 is half occupied on the special position of a $C_2$ rotation axis, bisecting the O1–Zn–O1$^{vi}$ angle, Fig. 3a), two triply bridging ($\mu_3$) hydroxide ligands and one fully deprotonated $BPPA^{3-}$ ligand. Thereby, a $\{Zn2O_4\}$ tetrahedron, a $\{Zn1O_5\}$ trigonal bipyramid and a $\{Zn3O_6\}$ octahedron are formed (Fig. 3 and Fig. S27 in ESI†). For the five-coordinated Zn1 atom the difference between the two largest angles yields $\tau = (172.9 - 128.6)°/60° = 0.74$, which is closer to the value for a trigonal bipyramid ($\tau = 1$) than for a square pyramid ($\tau = 0$).[70] The two oxygens from the –COO⁻ group bridge two Zn ions and the –PO₃²⁻ group is coordinated to four Zn ions (Fig. 3a). Overall the $BPPA^{3-}$ ligand bridges between six Zn atoms. The $\{ZnO_x\}$ polyhedra are edge- and corner-sharing (Fig. 3c and S28 in ESI†). The $\{ZnO_x\}$ ($x = 4$–6) polyhedra with their bridging $\mu_3$-OH⁻, $\mu_4$-PO₃²⁻ and $\mu_2$-COO⁻ groups are arranged in layers (parallel to the $bc$ plane) (Fig. 3b and c) and these layers are connected by the biphenyl part of the ligand to a 3D network (Fig. 3d).

The phosphorus atom in **5** has four different substituents, thus, is asymmetric and $R$-configured in the investigated single crystal. Only P atoms of the same handedness are assembled in the layers of **5** giving the non-centrosymmetric point group $C_2$ (Flack parameter 0.030(3)).[68] Circular dichroism (CD) spectra of **5** performed with KBr pellets (0.05 wt% of **5** according to a previously published protocol for solid state CD)[71] (Fig. S33 in ESI†) do not contain any significant spectral features that would indicate enantiomeric excess of either one of the two possible enantiomers of **5**. Therefore, as previously observed for other cases of spontaneous resolution,[72,73] the overall crystal ensemble is racemic.

Zn compounds with 4-phosphonate-biphenyl-3′,5′-dicarboxylate as a linker and templating amine bases are known[74] but do not show the same layer motif. A zinc complex with the shorter 4-phosphonate-benzoate ligand $PPA^{3-}$ has a zeolite-like structure, in which zigzag chains exist and $\{Zn_4O\}$ tetrahedra are coordinated by $PPA^{3-}$.[75]
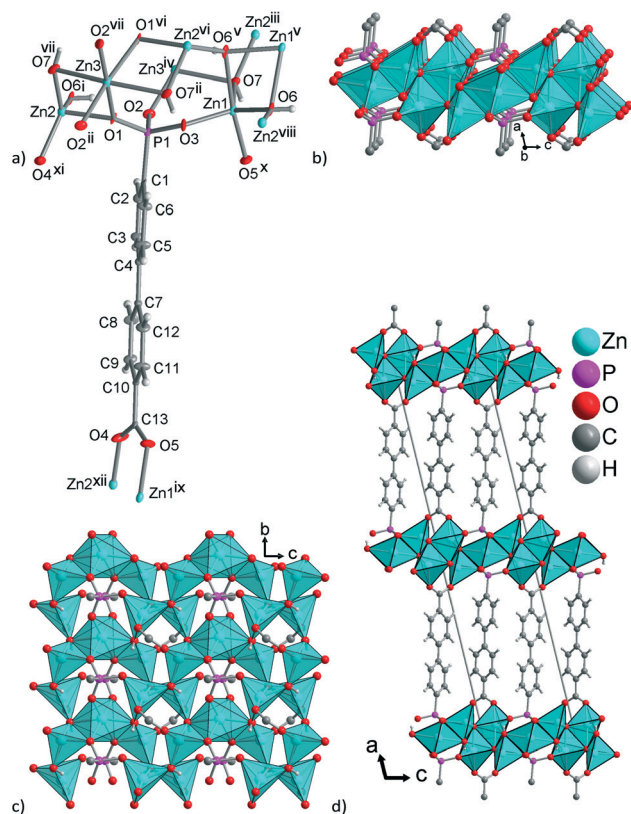
**Fig. 3** (a) Expanded asymmetric unit of **5** (70% thermal ellipsoids, except for C with 50% and H with arbitrary radii) and (b, c) layers of zinc ions, bridged by hydroxido, carboxylate and phosphonate groups, {Zn$_5$($\mu_3$-OH)$_4$($\mu_4$-O$_3$PC–)$_2$(–CO$_2$-$\mu_2$)$_2$} with the {ZnO$_x$} polyhedra presented as such. (d) Projection of the three-dimensional packing on the *ac* plane. Symmetry transformations: i = *x*, *y*, 1 + *z*; ii = *x*, 1 + *y*, *z*; iii = *x*, *y*, −1 + *z*; iv = *x*, −1 + *y*, *z*; v = −*x*, *y*, −*z*; vi = −*x*, *y*, 1 − *z*; vii = −*x*, 1 + *y*, 1 − *z*; viii = −*x*, −1 + *y*, 1 − *z*; ix = 1/2 − *x*, 1/2 + *y*, 1 − *z*; x = 1/2 − *x*, −1/2 + *y*, 1 − *z*; xi = 1/2 − *x*, 1/2 + *y*, 2 − *z*; xii = 1/2 − *x*, −1/2 + *y*, 2 − *z*. Further figures also showing the O–H⋯O H-bonds are given in ESI† as Fig. S27–S29. Selected distances and angles are given in Table 1.
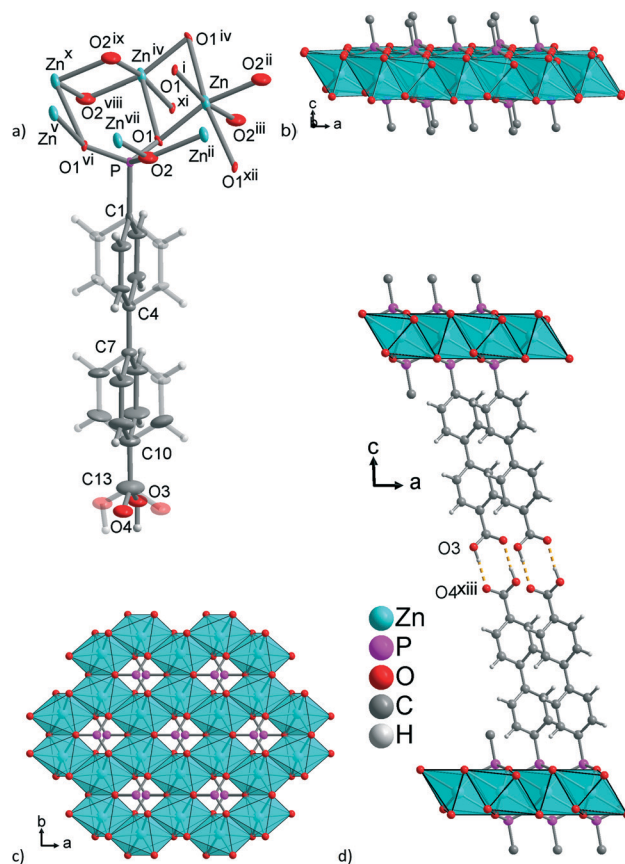


**Fig. 4** (a) Expanded asymmetric unit of the zinc compound **6** (isostructural with the cobalt compound **9**) (50% thermal ellipsoids) and (b, c) layers of zinc ions, bridged by phosphonate groups, {Zn($\mu_6$-O$_3$PC–)} with the {ZnO$_6$} octahedra shown as polyhedra. (d) Section of the three-dimensional supramolecular packing through the tail-to-tail hydrogen-bonding arrangement (orange dashed lines) of the carboxylic acid groups. Symmetry transformations: i = −*x* + 1, *y*, −*z* + 1; ii = −*x* + 3/2, −*y* + 3/2, −*z* + 1; iii = *x* − 1/2, *y* + 1/2, *z*; iv = −*x* + 1/2, −*y* + 3/2, −*z* + 1; v = −*x* + 1, −*y* + 1, −*z* + 1; vi = *x*, −*y* + 1, *z*; vii = *x* + 1/2, *y* − 1/2, *z*; viii = −1 + *x*, *y*, *z*; ix = 1 − *x*, *y*, 1 − *z*; x = −1/2 + *x*, −1/2 + *y*, *z*; xi = −1/2 + *x*, 3/2 − *y*, *z*; xii = 1/2 + *x*, 3/2 − *y*, *z*; xiii = 2 − *x*, 1 − *y*, −*z*. Selected distances and angles are given in Table 2.

The zinc compound [Zn($\mu_6$-O$_3$P–(C$_6$H$_4$)$_2$–CO$_2$H)] (**6**) was obtained from a 1:1 molar ratio of Zn(NO$_3$)$_2$·4H$_2$O and H$_3$BPPA in water without any modifier. No deprotonating or buffer agent was added. The structure of **6** consists of Zn(II) ions that are coordinated by the HBPPA$^{2-}$ ligand with only the phosphono group deprotonated (–PO$_3^{2-}$) and the carboxyl group still protonated (–COOH). The asymmetric unit contains a unique zinc atom and the ligand HBPPA$^{2-}$ on special positions with half-occupancy. This leads to a crystallographically induced disorder of the ligand over two split-positions (Fig. 4a).

In the cobalt structure with the shorter 4-phosphono benzoic acid ligand,[52] which is analogous to compound **9** (see below), the same disorder of the phenyl ring and of the –COOH was observed. The Zn atom is coordinated by six oxygen atoms in a distorted octahedron with four shorter bonds in the equatorial plane and two longer axial bonds. The oxygen atoms of $\mu_6$-PO$_3^{2-}$ coordinate to six zinc ions with each O atom bridging two zinc ions (Fig. 4a). The distorted {ZnO$_6$}

octahedra are edge-sharing and form a flat honeycomb layer parallel to the *ab* plane (Fig. 4b and c). The 2D-{Zn($\mu_6$-O$_3$PC–)} layers are connected by the biphenyl-carboxylic acid part of the ligand to a supramolecular 3D network through the carboxylic acid groups which are oriented towards each other with the typical tail-to-tail arrangement, also known as R$_2^2$(8)-motif in the Etter-notation (Fig. 4d and Table S5 in ESI†).[76]

Similarly compound [Co($\mu_6$-O$_3$P–(C$_6$H$_4$)$_2$–CO$_2$H)] (**9**) was prepared from an equimolar ratio of CoCl$_2$ and H$_3$BPPA in water. The single-crystal data set of **9** was not of sufficient quality to present a publishable structure determination. Yet, the isostructural nature of **6** and **9** could be established and also confirmed by comparison of the powder X-ray diffractograms (see Fig. S24 in ESI†).

The cadmium compound [Cd$_3$($\mu_6$-O$_3$P–(C$_6$H$_4$)$_2$–CO$_2$-$\mu_2$)($\mu_6$-O$_3$P–(C$_6$H$_4$)$_2$–CO$_2$-$\mu_3$)] (**7**) was obtained from a 3:2 molar ratio

**Table 1** Selected distances (Å) and angles (°) in **5**$^a$

| | | | |
|---|---|---|---|
| Zn1–O3 | 1.940(4) | Zn2–O4$^{xi}$ | 1.909(5) |
| Zn1–O5$^x$ | 2.010(5) | Zn2–O6$^i$ | 1.970(4) |
| Zn1–O6 | 2.007(4) | Zn2–O7$^{vii}$ | 1.974(4) |
| Zn1–O6$^v$ | 2.256(5) | Zn3–O1 | 2.133(4) |
| Zn1–O7 | 2.014(5) | Zn3–O2$^{ii}$ | 2.013(5) |
| Zn2–O1 | 1.991(4) | Zn3–O7$^{ii}$ | 2.264(4) |
| | | | |
| O3–Zn1–O6$^v$ | 110.82(18) | O4$^{xi}$–Zn2–O1 | 103.41(19) |
| O3–Zn1–O5$^x$ | 96.31(18) | O6$^i$–Zn2–O1 | 104.64(19) |
| O6–Zn1–O5$^x$ | 99.97(18) | O7$^{vii}$–Zn2–O1 | 89.09(18) |
| O3–Zn1–O7 | 116.73(18) | O2$^{ii}$–Zn3–O2$^{vii}$ | 97.0(3) |
| O6–Zn1–O7 | 128.57(19) | O2$^{ii}$–Zn3–O1 | 86.30(16) |
| O5$^x$–Zn1–O7 | 93.40(19) | O2$^{vii}$–Zn3–O1 | 175.21(18) |
| O3–Zn1–O6$^v$ | 90.79(17) | O1$^{vi}$–Zn3–O1 | 90.6(2) |
| O6–Zn1–O6$^v$ | 77.4(2) | O2$^{ii}$–Zn3–O7$^{ii}$ | 98.01(16) |
| O5$^x$–Zn1–O6$^v$ | 172.90(17) | O2$^{ii}$–Zn3–O7$^{vii}$ | 90.37(16) |
| O7–Zn1–O6$^v$ | 83.34(17) | O1–Zn3–O7$^{ii}$ | 92.64(16) |
| O4$^{xi}$–Zn2–O6$^i$ | 110.3(2) | O1$^{vi}$–Zn3–O7$^{ii}$ | 78.43(15) |
| O4$^{xi}$–Zn2–O7$^{vii}$ | 126.2(2) | O2$^{ii}$–Zn3–O7$^{vii}$ | 90.37(16) |
| O6$^i$–Zn2–O7$^{vii}$ | 116.62(19) | O2$^{vii}$–Zn3–O7$^{vii}$ | 98.01(16) |
| | | O1–Zn3–O7$^{vii}$ | 78.32(15) |
| Zn1–O6–Zn2$^{iii}$ | 127.5(2) | O1$^{vi}$–Zn3–O7$^{vii}$ | 92.64(16) |
| Zn2–O1–Zn3 | 97.19(17) | O7$^{ii}$–Zn–O7$^{vii}$ | 167.4(2) |
| Zn1–O7–Zn3$^{iv}$ | 110.38(19) | | |

$^a$ Symmetry transformations: i = $x$, $y$, 1 + $z$; ii = $x$, 1 + $y$, $z$; iii = $x$, $y$, −1 + $z$; iv = $x$, −1 + $y$, $z$; v = −$x$, $y$, −$z$; vi = −$x$, $y$, 1 − $z$; vii = −$x$, 1 + $y$, 1 − $z$; viii = −$x$, −1 + $y$, 1 − $z$; ix = 1/2 − $x$, 1/2 + $y$, 1 − $z$; x = 1/2 − $x$, −1/2 + $y$, 1 − $z$; xi = 1/2 − $x$, 1/2 + $y$, 2 − $z$; xii = 1/2 − $x$, −1/2 + $y$, 2 − $z$.



**Scheme 4** Octahedron and trigonal prism with enhanced triangular faces and relevant parameters for the assessment of their relationship. $\phi$ is the twist angle between the enhanced triangles around the $C_3$ axis.

polyhedra in compound **7** can be regarded as distorted trigonal prisms (see average values in Scheme 5 from the data in Table S12 in ESI†).

The –PO$_3^{2-}$ oxygens bridge between five Cd atoms, while the –COO$^-$ groups bridge either two or three Cd atoms (Fig. 5a, Scheme 3 and Fig. S31 in ESI†). Overall, the BPPA$^{3-}$ ligand bridges seven or eight Cd atoms. The edge- and vertex-sharing {CdO$_6$} trigonal prisms with their bridging $\mu_5$-PO$_3^{2-}$ and $\mu_2/\mu_3$-COO$^-$ groups are arranged in flat layers (parallel to

**Table 2** Selected distances (Å) and angles (°) in **6**$^a$

| | | | |
|---|---|---|---|
| Zn–O1 | 1.931(4) | Zn–O1$^{xii}$ | 2.620(4) |
| Zn–O2$^{iii}$ | 1.973(6) | | |
| | | | |
| O1–Zn–O1$^i$ | 93.2(3) | O1$^{iv}$–Zn–O1$^{xii}$ | 171.1(3) |
| O1–Zn–O2$^{ii}$ | 162.8(3) | O1–Zn–O1$^{xii}$ | 82.8(4) |
| O1–Zn–O2$^{iii}$ | 93.7(2) | Zn–O1–Zn$^{iv}$ | 76.6(2) |
| O2$^{ii}$–Zn–O2$^{iii}$ | 84.2(4) | Zn$^{ii}$–O2–Zn$^{vii}$ | 95.8(4) |
| O1$^i$–Zn–O1$^{xii}$ | 103.4(3) | | |

$^a$ Symmetry transformations: i = −$x$ + 1, $y$, −$z$ + 1; ii = −$x$ + 3/2, −$y$ + 3/2, −$z$ + 1; iii = $x$ − 1/2, $y$ + 1/2, $z$; iv = −$x$ + 1/2, −$y$ + 3/2, −$z$ + 1; vii = $x$ + 1/2, $y$ − 1/2, $z$; xii = 1/2 + $x$, 3/2 − $y$, $z$.

of Cd(OAc)$_2$ and H$_3$BPPA in water in the presence of oxalic acid (added to allow stable pH values).

In the crystal structure of **7**, the asymmetric unit consists of three different Cd atoms and two fully deprotonated BPPA$^{3-}$ ligands. The Cd atoms are coordinated by six oxygen atoms from both $\mu_2$- and $\mu_3$-COO$^-$ and $\mu_5$-PO$_3^{2-}$ groups (Fig. 5a).

Significant distortion from classical octahedral towards trigonal-prismatic (TP) geometry around Cd is clearly revealed in the structure of **7** (see Cd-polyhedra in Table S12 in ESI†). An idealized octahedron has two exactly parallel, staggered equilateral triangles and all edges of side $s$ (Scheme 4). Consideration of the angular parameters $\theta$, $\rho$ and $\omega$ (Scheme 5) in the comparison between octahedral and trigonal prismatic limiting structures[77,78] indicates that the Cd
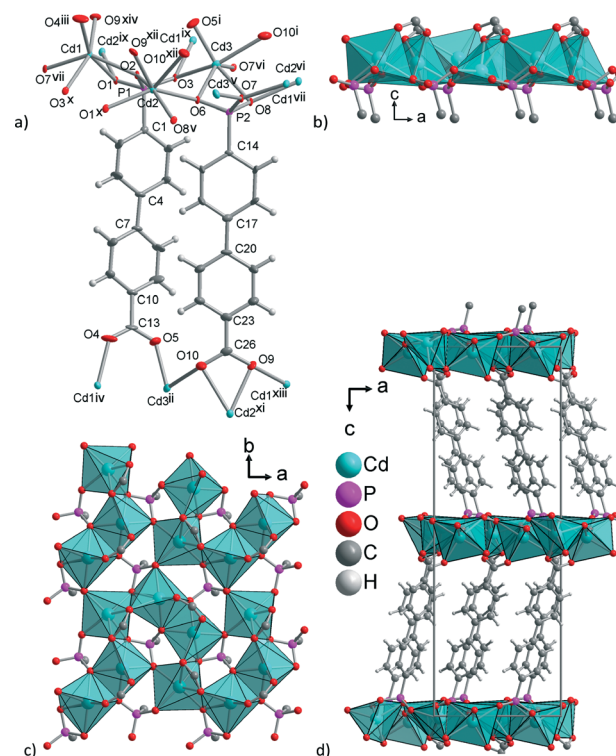


**Fig. 5** (a) Expanded asymmetric unit of the cadmium compound **7** (Cd and P 70%, C and O 50% thermal ellipsoids) and (b, c) layers of cadmium ions, bridged by phosphonate and carboxylate groups, {Cd$_3$($\mu_5$-O$_3$PC–)$_2$(–CO$_2$-$\mu_2/\mu_3$)$_2$} with the {CdO$_6$} trigonal prisms depicted as polyhedra. (d) Projection of the three-dimensional packing on the $ac$ plane. Symmetry transformations: i = 1/2 − $x$, $y$, 1/2 + $z$; ii = 1/2 − $x$, $y$, −1/2 + $z$; iii = −$x$, 2 − $y$, 1/2 + $z$; iv = −$x$, 2 − $y$, −1/2 + $z$; v = −1/2 + $x$, 1 − $y$, $z$; vi = 1/2 − $x$, 2 − $y$, −1/2 + $z$; vii = $x$, −1 + $y$, $z$; ix = 1/2 + $x$, 2 − $y$, $z$; x = −1/2 + $x$, 2 − $y$, $z$; xi = −$x$, 1 − $y$, −1/2 + $z$; xii = −$x$, 1 − $y$, 1/2 + $z$; xiii = 1/2 − $x$, −1 + $y$, −1/2 + $z$; xiv = 1/2 − $x$, 1 + $y$, 1/2 + $z$. Selected distances are given in Table 3. Angles are listed in Table S6 in ESI†.
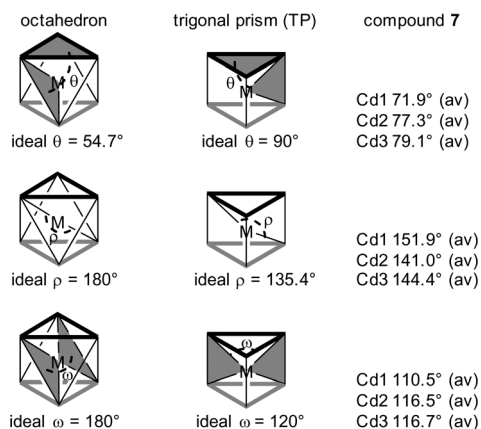
**Scheme 5** Angular parameters involved in the comparison between the octahedral and trigonal-prismatic limiting structures. $\theta$ = angle between the mean plane of the two $O_3$ triangles and the chelate planes defined by the metal and each pair of near eclipsed O vertices. $\rho$ = angle between the metal and *trans* O-donor sites. $\omega$ = angle between the triangular faces defined by the metal and near eclipsed O atoms. The angle for Cd$i$ is the average of three angles, which are listed in Table S12 in ESI.†

**Table 3** Selected distances (Å) in **7**[a]

| | | | |
|---|---|---|---|
| Cd1–O1 | 2.370(7) | Cd2–O8$^{v}$ | 2.273(8) |
| Cd1–O2 | 2.294(7) | Cd2–O9$^{xii}$ | 2.387(9) |
| Cd1–O3$^{x}$ | 2.359(8) | Cd2–O10$^{xii}$ | 2.458(9) |
| Cd1–O4$^{iii}$ | 2.177(9) | Cd3–O3 | 2.328(8) |
| Cd1–O7$^{vii}$ | 2.263(7) | Cd3–O5$^{i}$ | 2.132(9) |
| Cd1–O9$^{xiv}$ | 2.406(9) | Cd3–O6 | 2.324(8) |
| Cd2–O1$^{x}$ | 2.286(8) | Cd3–O7$^{vi}$ | 2.201(7) |
| Cd2–O2 | 2.226(7) | Cd3–O8 | 2.328(8) |
| Cd2–O6 | 2.289(8) | Cd3–O10$^{i}$ | 2.541(10) |

[a] For angles see Table S6 in ESI. Symmetry transformations: i = 1/2 − x, y, 1/2 + z; ii = 1/2 − x, y, −1/2 + z; iii = −x, 2 − y, 1/2 + z; v = −1/2 + x, 1 − y, z; vi = 1/2 + x, 1 − y, z; vii = x, −1 + y, z; ix = 1/2 + x, 2 − y, z; x = −1/2 + x, 2 − y, z; xii = −x, 1 − y, 1/2 + z; xiii = 1/2 − x, −1 + y, −1/2 + z; xiv = 1/2 − x, 1 + y, 1/2 + z.

the *ab* plane) (Fig. 5b and c) and these layers are connected by the biphenyl part of the ligand to a 3D network (Fig. 5d).

Compound **7** crystallizes in the non-centrosymmetric orthorhombic space group $Pca2_1$. The non-centrosymmetric packing (Flack parameter 0.007(9))[68] originates from the identical orientation of the phosphonato ends (or the carboxylato ends, respectively) of the $^{2-}O_3P–(C_6H_4)_2–CO_2^{-}$ linkers along the crystallographic *c* axis (Fig. 5d).

Five edge- and vertex-sharing $\{CdO_6\}$ polyhedra form a pentagon, which assembles into a 2D **mcm**-net (Fig. 6a).[79] In its regular form this pentagon tiling consists of two kinds of vertices ($5^3$ and $5^4$, connecting 3 or 4 pentagons, respectively), two kinds of edges and one kind of face.

The mercury(I) compound with the sum formula [Hg($\mu_3$-HO$_3$P–(C$_6$H$_4$)$_2$–CO$_2$H)] (**8**) was obtained from an equimolar ratio of mercury(II) acetate, Hg(OAc)$_2$, and H$_3$BPPA in water in the presence of oxalic acid to allow stable pH values. In **8**, the mercury oxidation state assignment depends on the pres-
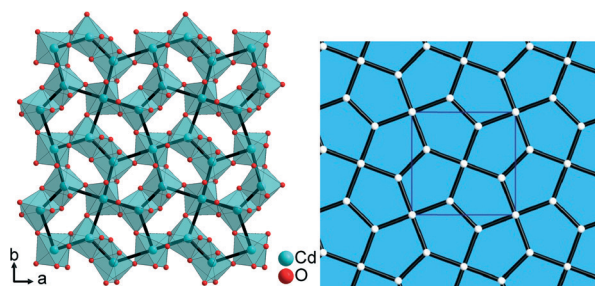


**Fig. 6** Left: Layer of $\{CdO_6\}$ polyhedra in **7** with the Cd atoms connected by black lines to illustrate the pentagonal **mcm** tiling. Right: **mcm** net from http://rcsr.net/layers/mcm.[79]

ence or absence of the calculated proton on the phosphonato group, $^{-}HO_3P$.

The phosphonate group of the ligand remains singly protonated (or is only singly deprotonated), that is, –PO$_3$H$^{-}$ with the O3 atom carrying the H atom. The carboxyl group remains protonated as is clearly evidenced by the tail-to-tail hydrogen-bonding arrangement. The H3 atom on O3 of –PO$_3$H$^{-}$ could be found and refined with $U_{iso}(H)$ = $1.5U_{eq}(O)$ and the DFIX restraint 0.90 ± 0.05 Å.

Bond valence sum calculations[80,81] done on the Hg atom of **8** gave a value of 0.83 when assuming a valence of 1 and a value of 1.00 when assuming a valence of 2. The calculated values support the valence of 1.

In the structure of **8**, two mercury ions form a handle with $C_2$-symmetry-related Hg atoms at a Hg–Hg distance of 2.5116(14) Å, presumably the well-known dinuclear Hg$_2^{2+}$ dication. A possible Hg$_2^{4+}$ cation is rare. The di-mercury(II) complex bis($\mu$-$P,N$-1-benzyl-2-imidazolyl-diphenylphosphine)($\mu$-$O,O'$-diperchloratedimercury(II) diperchlorate ($C_{44}H_{38}N_4O_{16}P_2$-$Cl_4Hg_2$) is one example,[82] but the Hg–Hg distance with 3.071(1) Å is longer than in **8**. The short Hg–Hg distance of ~2.5 Å falls in the distance range of 2.46–2.60 Å observed for a Hg(I)$_2^{2+}$ cation.[83]

Hence, we assume a Hg(I) oxidation state with single-deprotonated H$_3$BPPA ligand. The asymmetric unit contains one unique Hg atom and one H$_2$BPPA$^{-}$ ligand. Each Hg atom is coordinated by three oxygens from three different $^{-}HO_3P$-groups (Fig. 7a) with a severely distorted tripodal HgO$_3$ coordination, which is tilted with respect to the Hg–Hg bond (Fig. 7b and Fig. S32, ESI†). There is one short Hg1–O1 contact of 2.118(13) Å and two considerably longer contacts Hg1–O2$^{iii}$ = 2.566(16) Å and Hg1–O3$^{iv}$ = 2.729(15) Å (Table 4 and Fig. 7a). This coordination environment agrees with a classical L–Hg(I)–Hg(I)–L species. For Hg(II), a higher coordination number of four to eight is expected, whereas a coordination number of three for H(II) is very rare.[84] More importantly, no direct Hg–Hg bonds are found in coordination polymers of mercury(II).[84] For Hg$_2^{2+}$, there are several examples of complexes in the Cambridge Structure Database in which the overall coordination number of a Hg(I) atom is four.[85] Furthermore, an *in situ* reduction of Hg$^{2+}$ to Hg$_2^{2+}$ was also observed by Su *et al.*[85c]
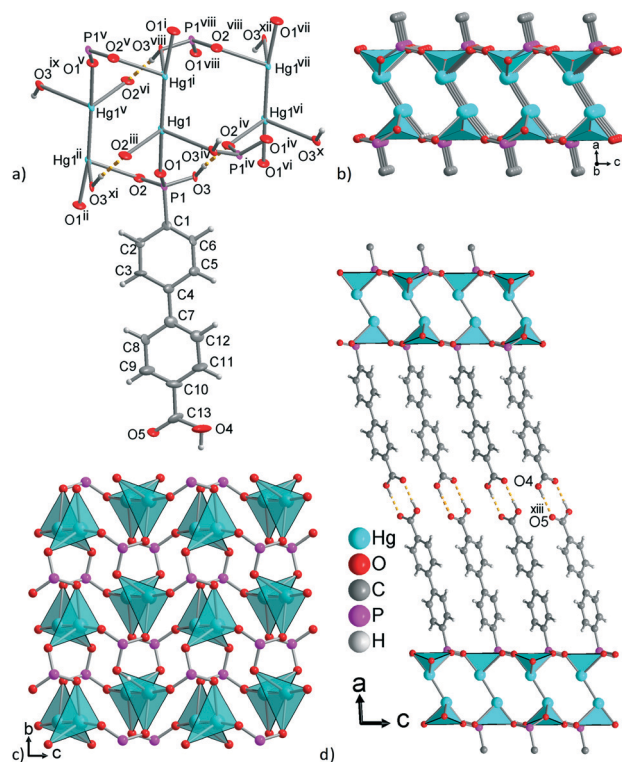
**Fig. 7** (a) Expanded asymmetric unit of **8** (Hg and P 70%, C and O 50% thermal ellipsoids; H bonds are orange dashed lines) and (b, c) layers of $Hg_2^{2+}$ handles, bridged by phosphonate groups, $\{Hg_2(\mu_3\text{-}HO_3PC\text{-})_2\}$ with the $\{HgO_3\}/\{Hg_2O_6\}$ depicted as polyhedra. (d) Section of the supramolecular three-dimensional packing through the tail-to-tail hydrogen-bonding arrangement (orange dashed lines) of the carboxylic acid groups. Symmetry transformations: i = 1 − x, y, 1/2 − z; ii = x, −y, 1/2 + z; iii = x, −y, −1/2 + z; iv = x, 1 − y, −1/2 + z; v = 1 − x, −y, 1 − z; vi = x, 1 + y, z; vii = 1 − x, 1 + y, 1/2 − z; viii = 1 − x, 1 − y, 1 − z; ix = 1 − x, −1 + y, 3/2 − z; x = x, 2 − y, −1/2 + z; xi = x, −1 + y, z; xii = 1 − x, 2 − y, 1 − z. Selected distances and angles are given in Table 4; hydrogen bonding interactions in Table S8 in ESI.†

**Table 4** Selected bond distances (Å) and angles (°) in **8**[a]

| | | | |
|---|---|---|---|
| Hg1–O1 | 2.118(13) | Hg1–O3[iv] | 2.729(15) |
| Hg1–O2[iii] | 2.566(16) | Hg1–Hg1[i] | 2.5116(14) |
| | | | |
| O1–Hg1–Hg1[i] | 171.7(4) | P1–O1–Hg1 | 133.6(9) |
| O1–Hg1–O2[iii] | 78.3(5) | P1–O2–Hg1[ii] | 120.1(8) |
| Hg1[i]–Hg1–O2[iii] | 108.9(3) | O3[iv]–Hg1–Hg1[i] | 101.3(3) |
| O3[iv]–Hg1–O2[iii] | 97.0(5) | | |

[a] Symmetry transformations: i = 1 − x, y, 1/2 − z; ii = x, −y, 1/2 + z; iii = x, −y, −1/2 + z; iv = x, 1 − y, −1/2 + z.

The phosphonate groups of six ligands (three on each Hg) are bridging the Hg–Hg handles to a flat 2D-$\{Hg_2(\mu_3\text{-}HO_3P\text{-})\}$ layer (Fig. 7b and c). These 2D-layers are connected by the biphenyl-carboxylic acid part of the ligand to a supramolecular 3D network through the carboxylic acid groups which are oriented towards each other in the tail-to-tail arrangement ($R_2^2(8)$-motif in the Etter-notation)[76] (Fig. 7d and S32, Table S8, ESI†).

A mixed-valent mercury complex with L-alanine, $[Hg_{12}(L\text{-}ala)_8(NO_3)_8]\cdot2H_2O$ showed a coordination environment for Hg similar to the one found for **8**.[86] A compound of mercury with a phosphono-carboxylate linker has been unknown.

There are seven entries in the Cambridge Structure Database, CSD, with a –P–O–Hg coordination, from which only two (AFIWES[87] and SARSAF[88]) contain phosphonates coordinated to Hg(ɪɪ) and of which none has Hg–Hg handles.

All metal-linker compound **5–9** share the layer motif for the $\{MO_x\}$ polyhedra. The driving force appears to be the separation of polar and nonpolar parts of molecules, which is a common packing motif.[89–91]

CH-π contacts between neighbouring biphenyl systems in **5–8** are listed in Tables S9–S11 in ESI† with angles and distances of significant interactions.

A listing of the dihedral angles in the BPPA linker in complexes **5–8** is given in Table S13 in the ESI.† With dihedral angles ranging from 0.1(6)° (**5**) to 2.0(2)° (**8**), the aryl systems are nearly co-planar (0°) to each other, favouring the π-electron delocalisation. The aryl-COO(H) angles vary from 2.0(2)° (**6, 7**) to 16.3(9)° (**5**), which is explained by the different state of protonation and coordination of the –COO group. Still, a close to planar geometry of the ligand is observed in all complexes.

## Hydrothermal stability

The noteworthy water stability of the complexes **5–9** has been investigated by long-time exposure of the complexes in water. IR and powder X-ray diffraction, PXRD, did not indicate any structural changes within months. Furthermore, the hydrothermal synthesis conditions (water at 180–200 °C) would not allow the formation of water-unstable structures.

The thermogravimetric behavior in Fig. 8 (detailed Fig. S19–S23 in ESI†) reveals a high thermal stability for **5** and **7**. The thermally stable ligand (m.p. >350 °C) contributes to the overall stability of the compounds through the strong metal-phosphonate coordination. The mass loss of ~5% in **4** (see Fig. S18 in ESI†) can be explained by a dehydration (−1H₂O,
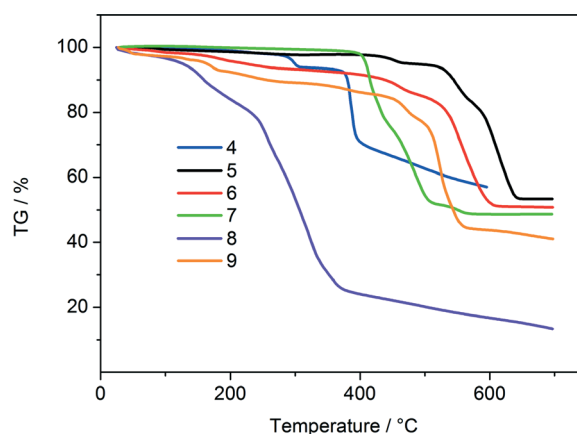


**Fig. 8** Thermogravimetric analysis (TGA) curves of compounds **4–9**.

18 g mol$^{-1}$, 6%) through the condensation of phosphonic acid groups to give anhydrides.[92]

Compounds **5** and **7**, where the ligand is fully deprotonated without a remaining –COOH group, start to decompose at ~400 °C. The isostructural compounds **6** and **9**, where only the phosphono group is deprotonated ($-PO_3^{2-}$) and the carboxyl group still protonated (–COOH), show a steady weight loss starting at ~150–200 °C, presumably first by a condensation ($-1H_2O$, 18 g mol$^{-1}$: 5.3% in **6** and **9**) followed by a decarboxylation ($-1CO_2$, 44 g mol$^{-1}$: 13% in **6**; 13.5% in **9**). The mercury compound **8** undergoes a rapid mass loss, starting already at ~100 °C, which can also be observed in other Hg complexes.[93] A decarboxylation is observed in the temperature range from 120 to 180 °C ($-1CO_2$, 45 g mol$^{-1}$, 9.5%). Hg complexes vaporize completely because of the high volatility of elemental Hg above 500 °C. Elemental Hg is formed by decomposition of intermediate HgO to its elements.

### Luminescence

Many organic molecules are only fluorescent in solution because in their solid-state they are subject to self-quenching with concomitant low quantum yield of their luminescence.[94] Immobilization/rigidification of organic molecules as linkers or as guest molecules in a solid framework like a coordination polymer[95] or MOF with $d^{10}$ metal ions such as Zn$^{2+}$ and Cd$^{2+}$ will reduce non-radiative relaxation caused by free rotation and vibration and, therefore, lead to stronger emissions.[96,97]

The emission spectrum of **4** (Fig. 9) shows a broad band with a maximum at around 365 nm when excited at 316 nm. The spectrum is comparable to that of dihydroxybiphenyls, such as 4,4′-dihydroxybiphenyl ($\lambda_{max}$ = 354 nm) and 2,2′-di-

hydroxybiphenyl ($\lambda_{max}$ = 356 nm) and many other previously reported substituted biphenyl systems ($\lambda_{max}$ = 318–420 nm).[98]

It is well documented that the luminescence observed in MOFs or coordination polymers of transition metal ions without unpaired electrons (such as Cd$^{2+}$ and Zn$^{2+}$) are typically ligand centered.[99,100] The emission spectra of the Zn compound **5** ($\lambda_{ex}$ = 354 nm), the Cd compound **7** ($\lambda_{ex}$ = 350 nm), the Hg compound **8** ($\lambda_{ex}$ = 345 nm) and the Co compound **9** ($\lambda_{ex}$ = 360 nm) also exhibit broad emission bands in the visible range at 410–420 nm suggesting that the luminescence in all compounds originate from the electronic transitions of the ligand. The emission spectra of the complexes are red shifted compared to that of the ligand, **4**, due to the different coordination and crystal packing interactions. The positions of the emission bands may be explained by different dihedral angles of the aromatic rings in the ligand and the complexes. Smaller dihedral angles result in enhanced π electron interactions, which in turn shift the emission bands to lower energies.[101] Although the dihedral angle in the ligand **4** is not known, in the metal compounds it is consistently very close to 0°: 0.1(6)° (**5**), 1.5(1)° (**6**), 0.5(2)° (**7**) and 2.0(2)° (**8**). Even though the dihedral angles in the excited states cannot be determined, it may be assumed that due to the crystal in rigid structures the conformations do not change significantly. To the best of our knowledge, no luminescent phosphonate–carboxylate compounds with Zn$^{2+}$, Hg$_2^{2+}$ and Cd$^{2+}$ ions have been reported so far.

## Conclusions

We have presented the crystal structures of five complexes with the new BPPA$^{3-}$ or HBPPA$^{2-}$ ligand. The new mixed-functional linker assumes (five) different metal–oxygen(ligand) coordination modes depending on the metal. Yet, all metal-linker compounds **5–9** share the common motif of {MO$_x$} polyhedra arranged in a mostly flat layer, which are connected by the biphenyl part, either directly or through tail-to-tail carboxyl groups. This way, polar and nonpolar parts of the molecules are separated, which is a common packing motif. In the flat {MO$_x$} layers in **6** and **7** the Zn and Cd metal nodes represent a honeycomb and an **mcm** net, respectively. Between the biphenyl groups, CH-π contacts are present (see ESI†). The coordination polyhedra of the Cd atoms in compound **7** were analyzed towards a trigonal-prismatic coordination environment. When the linker is fully deprotonated to BPPA$^{3-}$ the metal–ligand networks feature a high thermal stability of ~400 °C. When the carboxyl group is still protonated (–COOH in HBPPA$^{2-}$) a decarboxylation starts at ~150–200 °C, yet further decomposition only occurs above 400 °C. All compounds are very resistant against hydrolysis as they were synthesized in water at up to 200 °C and were stored in either water or air. The fluorescence emission of the H$_3$BPPA ligand is red shifted by about 50 nm upon deprotonation and metal complexation. It was our aim to demonstrate, that the combination of the phosphonato, $-PO_3^{2-}$
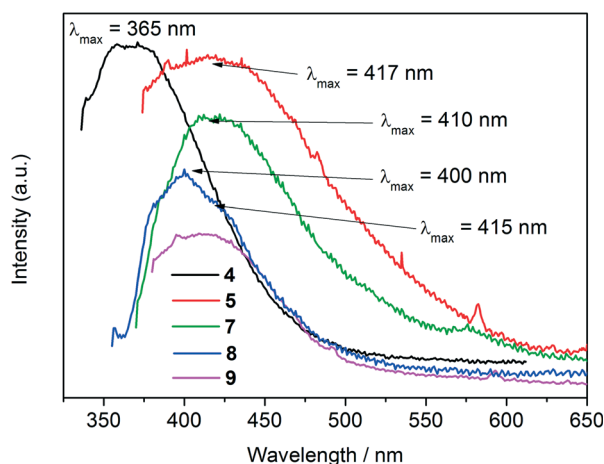


**Fig. 9** Solid-state luminescence spectra of complexes **5** ($\lambda_{ex}$ = 354 nm), **7** ($\lambda_{ex}$ = 350 nm), **8** ($\lambda_{ex}$ = 345 nm) and **9** ($\lambda_{ex}$ = 360 nm) in comparison with the spectrum of the ligand, **4** ($\lambda_{ex}$ = 316 nm). The spikes in the emission spectra are probably due to the lamp fluctuations or random pickup by the photomultiplier.

and carboxylato, –COO$^-$ function leads to hydrothermally stable network compounds.

## Experimental section

### Materials and methods

All reactants were commercially available and used without further purification. Doubly de-ionized (DI) water was used.

Elemental (CHN) analyses were performed on a Perkin Elmer CHN 2400. $^1$H, $^{13}$C and $^{31}$P NMR spectra were measured with a Bruker Avance DRX-200, Bruker Avance DRX-500 or Bruker Avance DRX-600. High-resolution electron-spray ionization mass spectra (HR-ESI-MS) were collected with a UHR-QTOF maXis 4G from Bruker Daltonics. Electron impact (EI) mass spectra were collected on a TSQ 7000 by Finnigan MAT. FT-IR spectra were recorded in ATR mode (Platinum ATR-QL, Diamond) on a Bruker TENSOR 37 IR spectrometer in the range of 4000–500 cm$^{-1}$. The absorbance bands have been described by the following terms: strong (s), medium (m), weak (w) and broad (br). Solid-state fluorescence spectra (2D) were obtained with a FluoroMax spectrometer from Horiba at room temperature. The samples were ground to a powder and pressed to fit securely in the sample holder (the mercury compound **8** has not been measured because of its toxicity). The reflection angle was set to be 60°. For thermogravimetric analysis (TGA) a Netzsch TG 209 F3 Tarsus was used, equipped with Al-crucible and a measurement range from 20 to 700 °C with a heating rate of 10 K min$^{-1}$ under inert atmosphere (N$_2$). Programmable ovens with heating and cooling ramps were from Memmert.

Melting points were determined using a Büchi Melting Point B540. For powder X-ray diffraction patterns (PXRD) a Bruker D2 Phaser powder diffractometer was used with flat panel low background sample holder, CuKα radiation ($\lambda$ = 1.5418 Å) at 30 kV, 10 mA, a scan speed of 0.2 s per step and a step size of 0.02° ($2\theta$).

Circular dichroism (CD) spectra of **5** were recorded on a J-810 spectropolarimeter (JASCO) with KBr pellets (0.05 wt% of **5**). To correct for linear anisotropy artifacts the KBr pellets were rotated during a measurement by the use of a motor-driven sample holder (20 rpm). The detector integration time was set to 16 s (scan rate: 20 nm min$^{-1}$). Each pellet was measured on the front and the reverse side. The resulting spectra (see Fig. S33 in ESI†) were averaged.

### Single crystal X-ray diffractometry

Suitable crystals were carefully selected under a polarizing microscope, covered in protective oil and mounted on a 0.05 mm cryoloop. *Data collection.* Bruker Kappa APEX2 CCD X-ray diffractometer with microfocus tube, Mo-Kα radiation ($\lambda$ = 0.71073 Å), multi-layer mirror system, $\omega$- and $\theta$-scans. Data collection with APEX II,[102] cell refinement with SMART, data reduction with SAINT[103] and experimental absorption correction with SADABS.[104] *Structure analysis and refinement*: The structures were solved by direct methods, SHELXS-97, refinement was done by full-matrix least squares on $F^2$ using the SHELX-97 program suite.[105] Non-hydrogen atoms were refined with anisotropic displacement parameters. Hydrogen atoms were positioned geometrically and refined using riding models [AFIX 43 for aromatic CH with C–H = 0.93 Å, AFIX 23 for CH$_2$ with C–H = 0.97 and $U_{iso}$(H) = 1.2$U_{eq}$(C), AFIX 137 for CH$_3$ with C–H = 0.96 Å and $U_{iso}$(H) = 1.5$U_{eq}$(C); AFIX 83 for –COOH and $U_{iso}$(H) = 1.5$U_{eq}$(O)]. Hydrogen atoms H1 and H7 on the OH groups in **5** have been freely refined in position and $U_{iso}$. Crystals of **5–9** were of very small size. It is known that very small crystals diffract weaker than larger crystals,[106] resulting in lower data quality and subsequent problems during refinement. Some of the *checkcif* alerts are due to the small crystal size, *e.g.*, poor data/parameter ratio (**6**, **7**). In **6** the disorder of the biphenyl moiety (treated with the PART command in SHELX) and –COOH group, which can have two different orientations, is causing level B alerts. The large residual electron density near the Hg atoms in **8** gave level A and B alerts. Nine of the 13 largest peaks of the residual electron density (including the three largest) are within 2 Å of the Hg atom in **8**. Crystal data and details on the structure refinement are given in Tables 5 and 6. Graphics were drawn with DIAMOND.[107] Analyses on the supramolecular C–H⋯O-, C–H⋯π- and π–π-stacking interactions were done with *PLATON* for Windows.[108] The crystallographic data have been deposited with the Cambridge Crystallographic Data Center (CCDC-numbers 1465329–1465334 for **3**, **6**, **8**, **5**, **2**, **7**, respectively).

### Syntheses

**4-Iodo-4′-biphenylcarboxylic acid (1).** According to a method of Merkushev and Yudina,[66] 10.0 g (0.05 mol) of 4-biphenylcarboxylic acid, 21.7 g (0.05 mol) of bis(trifluoroacetoxy)iodobenzene and 12.7 g (0.05 mol) of freshly ground iodine were placed in a 50 mL flask together with 20 mL of CCl$_4$. The deep-violet suspension was stirred for two hours at room temperature. The solid was filtered and washed with 3 × 10 mL of CCl$_4$. The resulting white powder was dried in vacuum (10$^{-1}$ mbar) to afford 13.3 g of pure product (82% yield). Mp = 310 °C (lit: 312 °C).[109] FT-IR (ATR) $\tilde{v}$/cm$^{-1}$ = 2976 (w, br), 2820 (w, br), 2668 (w), 2546 (w), 1827 (vs), 1677 (m), 1605 (m), 1572 (m), 1549 (m), 1514 (m), 1474 (m), 1424 (m), 1386 (m), 1321 (m), 1298 (m), 1280 (m), 1196 (s), 1177(m), 1123 (m), 1104 (m), 1062 (m), 1019 (m), 1010 (m), 996 (m), 954 (m), 871 (m), 818 (m), 767 (m), 744 (vs), 710 (m), 698 (m), 661 (m), 623 (m). $^1$H-NMR (200 MHz; DMSO-$d_6$) $\delta$/ppm = 7.53 (d, 2H, $J$ = 8.0 Hz), 7.79 (d, 2H, $J$ = 8.0 Hz), 7.84 (d, 2H, $J$ = 8.0 Hz), 8.01 (d, 2H, $J$ = 8.0 Hz). Spectra are given in Fig. S1 and S2 in the ESI.†

**4-Iodo-4′-biphenylcarboxylic acid methyl ester (2).** In a 50 mL glass flask 5.0 g (15.4 mmol) of **1** were suspended in 10 mL of a mixture of CCl$_4$ and N,N′-dimethylformamide (v : v = 1 : 1). Then 6.2 g (45.0 mmol) of K$_2$CO$_3$ were added to the suspension under stirring. A portion of 6.4 g (45.0 mmol) of methyliodide was added dropwise over one hour resulting in the formation of a yellowish, oily layer. The layers were

**Table 5**  Crystal data and structure refinement for **2** and **3**

| Compound | 2 | 3 |
|---|---|---|
| Chemical formula | $C_{14}H_{11}IO_2$ | $C_{18}H_{21}O_5P$ |
| $M_r$ | 338.13 | 348.32 |
| Crystal system | Orthorhombic | Triclinic |
| Space group | $Pca2_1$ | $P\bar{1}$ |
| Temperature (K) | 150 | 296 |
| $a$ (Å) | 6.0355 (4) | 8.094(2) |
| $b$ (Å) | 7.2980(4) | 8.186(2) |
| $c$ (Å) | 27.8833(18) | 13.626(4) |
| $\alpha$ (°) | 90 | 104.044(15) |
| $\beta$ (°) | 90 | 92.510(15) |
| $\gamma$ (°) | 90 | 99.071(14) |
| $V$ (Å$^3$) | 1228.18(13) | 861.7(4) |
| $Z$ | 4 | 2 |
| $\mu$ (mm$^{-1}$) | 2.593 | 0.18 |
| Crystal size (mm) | $0.10 \times 0.10 \times 0.05$ | $0.90 \times 0.20 \times 0.20$ |
| $T_{min}$, $T_{max}$ | 0.724, 0.745 | 0.620, 0.744 |
| No. measured, indep. and obs. [$I > 2\sigma(I)$] reflect. | 10 290, 2382, 2325 | 11 291, 3248, 2650 |
| $R_{int}$ | 0.049 | 0.053 |
| $(\sin\theta/\lambda)_{max}$ (Å$^{-1}$) | 0.624 | 0.613 |
| $R_1$ [$F^2 > 2\sigma(F^2)$], w$R_2$ $(F^2)$,[b] $S$[c] | 0.030, 0.099, 1.24 | 0.060, 0.175, 1.07 |
| No. of reflect./restraints/parameters | 2382/1/155 | 3248/0/220 |
| Weight. scheme w; $a/b$[d] | 0.050/0.6335 | 0.0925/0.6193 |
| Max./min. $\Delta\rho$ (e Å$^{-3}$)[a] | 0.81, −0.82 | 0.53, −0.47 |
| Absolute structure (Flack) parameter[e] | 0.080(17) | — |

[a] Largest difference peak and hole. [b] $R_1 = [\sum(||F_o| - |F_c||)/\sum|F_o|]$; w$R_2 = [\sum[w(F_o^2 - F_c^2)^2]/\sum[w(F_o^2)^2]]^{1/2}$. [c] Goodness-of-fit, $S = [\sum[w(F_o^2 - F_c^2)^2]/(n - p)]^{1/2}$. [d] w $= 1/[\sigma^2(F_o^2) + (aP)^2 + bP]$ where $P = (\max(F_o^2 \text{ or } 0) + 2F_c^2)/3$. [e] Ref. 68.

**Table 6**  Crystal data and structure refinement for **5**–**8**

| Compound | 5 | 6 | 7 | 8 |
|---|---|---|---|---|
| Chemical formula | $C_{26}H_{20}O_{14}P_2Zn_5$ | $C_{13}H_9O_5PZn$ | $C_{26}H_{16}Cd_3O_{10}P_2$ | $C_{13}H_{10}HgO_5P$ |
| $M_r$ | 945.31 | 341.54 | 887.53 | 477.77 |
| Crystal system | Monoclinic | Monoclinic | Orthorhombic | Monoclinic |
| Space group | $C2$ | $C2/m$ | $Pca2_1$ | $C2/c$ |
| Temperature (K) | 173 | 173 | 173 | 173 |
| $a$ (Å) | 32.8388(12) | 5.2848(12) | 9.3961(7) | 59.003(11) |
| $b$ (Å) | 5.3763(19) | 8.1031(18) | 9.5450(7) | 5.4907(9) |
| $c$ (Å) | 7.913(3) | 27.371(6) | 27.3230(19) | 7.8375(12) |
| $\beta$ (°) | 103.531(11) | 91.766(12) | 90 | 93.644(9) |
| $V$ (Å$^3$) | 1358.2(9) | 1171.6(5) | 2450.5(3) | 2534.0(7) |
| $Z$ | 2 | 4 | 4 | 8 |
| $\mu$ (mm$^{-1}$) | 4.55 | 2.25 | 2.77 | 12.29 |
| Crystal size (mm) | $0.10 \times 0.01 \times 0.01$ | $0.03 \times 0.03 \times 0.03$ | $0.10 \times 0.07 \times 0.05$ | $0.01 \times 0.01 \times 0.01$ |
| $T_{min}$, $T_{max}$ | 0.502, 0.748 | 0.724, 0.745 | 0.685, 0.747 | 0.515, 0.746 |
| No. measured, indep. and obs. [$I > 2\sigma(I)$] reflect. | 8001, 3360, 2930 | 5207, 1106, 912 | 48 627, 4301, 4281 | 11 056, 2121, 1633 |
| $R_{int}$ | 0.060 | 0.054 | 0.043 | 0.089 |
| $(\sin\theta/\lambda)_{max}$ (Å$^{-1}$) | 0.703 | 0.594 | 0.595 | 0.594 |
| $R_1$ [$F^2 > 2\sigma(F^2)$], w$R_2$ $(F^2)$,[b] $S$[c] | 0.041, 0.085, 1.01 | 0.068, 0.163, 1.05 | 0.032, 0.077, 1.13 | 0.070, 0.176, 1.03 |
| No. of reflections/restraints/parameters | 3360/1/220 | 1106/0/129 | 4301/1/310 | 2121/0/155 |
| Weight. scheme w; $a/b$[d] | 0.0302/0 | 0.0504/40.479198 | 0.008/37.947201 | 0.0831/363.958771 |
| Max./min. $\Delta\rho$ (e Å$^{-3}$)[a] | 1.67, −1.09 | 3.63, −1.72 | 1.73, −2.15 | 8.07, −3.81 |
| Absolute structure (Flack) parameter[e] | 0.030(3) | — | 0.007(9) | — |

[a] Largest difference peak and hole. [b] $R_1 = [\sum(||F_o| - |F_c||)/\sum|F_o|]$; w$R_2 = [\sum[w(F_o^2 - F_c^2)^2]/\sum[w(F_o^2)^2]]^{1/2}$. [c] Goodness-of-fit, $S = [\sum[w(F_o^2 - F_c^2)^2]/(n - p)]^{1/2}$. [d] w $= 1/[\sigma^2(F_o^2) + (aP)^2 + bP]$ where $P = (\max(F_o^2 \text{ or } 0) + 2F_c^2)/3$. [e] Ref. 68.

separated, the upper DMF layer was discarded, the solvent from the yellowish CCl$_4$ was removed in vacuum affording an off-white powder (5.0 g; 98% yield). Alternatively: In a 250 mL flask 2.5 g (7.9 mmol) of **1** were suspended in 100 mL of dry methanol. Conc. sulphuric acid (5 mL) was added and the suspension heated to reflux for 4 h. The solid was filtered and washed with plenty of water (>100 mL) to remove the acid and methanol. The product was dried to afford 2.4 g

(90%) of an off-white powder. Mp = 188 °C (lit.: 189 °C).[110] FT-IR (ATR) $\tilde{v}$/cm$^{-1}$ = 3399 (w, br), 2998 (w), 2944 (w), 2842 (w), 1936 (m), 1902 (m), 1781 (m), 1708 (s), 1602 (m), 1576 (m), 1474 (m), 1453 (m), 1431 (m), 1387 (m), 1330 (m), 1287 (m), 1269 (s), 1209 (m), 1186 (m), 1136 (m), 1110 (s), 1066 (m), 1018 (m), 995 (m), 949 (m), 860, 819 (s), 764 (vs), 697 (m), 662 (m), 622 (m), 588 (m). $^1$H-NMR (200 MHz, CDCl$_3$) $\delta$/ ppm = 3.92 (s, 3H), 7.34 (d, 2H, $J$ = 8.6 Hz), 7.59 (d, 2H, $J$ = 8.6 Hz), 7.77 (d, 2H, $J$ = 8.6 Hz), 7.08 (d, 2H, $J$ = 8.6 Hz). Spectra are given in Fig. S3 and S4 in ESI.†

**4-Diethylphosphono-4′-biphenylcarboxylic acid methyl ester (3).** In a two necked 50 mL flask 5.0 g (14.8 mmol) of **2** and 0.33 g (1.47 mmol) of anhydrous NiBr$_2$ were suspended in 10 mL of mesitylene. The suspension was placed under nitrogen and heated to 180 °C with constant stirring and refluxing. After one hour 3.5 g (22.3 mmol) of triethylphosphite were added drop-wise over 2 hours at 180 °C with the suspension changing its colour from greenish yellow to red and back again with each drop of triethylphosphite added. After refluxing another two hours for completion of the reaction the light green suspension was allowed to cool to room temperature. The excess of triethylphosphite and solvent was removed under reduced pressure. The resulting solid was washed with water and dried to afford 4.4 g (85% yield) of pure product. Mp = 77–79 °C. FT-IR (ATR) $\tilde{v}$/cm$^{-1}$ = 3785 (w), 2969 (w), 2911 (w), 1637 (w), 1593 (w), 1521 (w), 1428 (m), 1329 (m), 1250 (s), 1198 (m), 1091 (m), 1032 (m), 1010 (m), 962 (m), 824 (w), 768 (m), 686 (m), 611 (vs). $^1$H-NMR (500 MHz, DMSO-$d_6$) $\delta$/ppm = 1.22 (t, 6H), 3.87 (s, 3H), 4.01 (q, 4H), 7.33–8.35 (m, 8H). $^{13}$C-NMR (125.7 MHz, DMSO-$d_6$) $\delta$/ppm = 16.5 (–CH$_3$), 39.8 (–CH$_2$–), 52.5 (O–CH$_3$), 62.1 (O–CH$_3$), 127.6 (d), 130.1 (d), 132.1 (d), 142.5, 143.3 (aromatic C), 176.5 (–COOH). $^{31}$P{H}-NMR (121.5 MHz, DMSO-$d_6$) $\delta$/ppm = 17.53. Spectra are given in Fig. S5–S8 in ESI.† EI-MS(+) at 100 °C (M = C$_{18}$H$_{21}$O$_5$P 348.11 $m/z$ (%) 348 (15) [M], 320 (28) [M–C$_2$H$_4$]$^+$, 292 (41) [M–C$_2$H$_5$–C$_2$H$_4$]$^+$, 261 (22) [M–C$_2$H$_4$–C$_2$H$_3$O$_2$]$^+$, 152 (65) [M–PO$_3$(C$_2$H$_5$)$_2$–CO$_2$CH$_3$ = C$_{12}$H$_8$]$^+$. Calcd. for C$_{18}$H$_{21}$O$_5$P·H$_2$O (366.35 g mol$^{-1}$): C 59.01, H 6.33%. Found C 58.79, H 5.99%.

**4-Phosphonato-4′-biphenylcarboxylic acid (4), H$_3$BPPA.** In a 100 mL glass flask 1.0 g (2.87 mmol) of **3** were suspended in 15 mL of 37% hydrochloric acid and refluxed for 20 h. The off-white product was filtered and washed with plenty of water to remove any residual hydrochloric acid from the product. The product was dried to give 0.74 g (93%) of **4**. Mp > 350 °C (decomp.). FT-IR (ATR) $\tilde{v}$/cm$^{-1}$ = 3324 (w, b), 2955 (w, br), 2849 (w, br), 2677 (m), 2557 (m), 2166 (m), 1935 (m), 1808 (m), 1677 (vs), 1605 (m), 1574 (w), 1550 (w), 1429 (m), 1391 (m), 1302 (m), 1214 (m), 1179 (m), 1145 (m), 1102 (m), 1002 (vs), 946 (m), 868 (m), 831 (m), 799 (m), 771 (m), 755 (m), 722 (m), 689 (m), 577 (vs). $^1$H-NMR (200 MHz, DMSO-$d_6$) $\delta$/ppm = 7.70–7.90 (m, 6H), 8.04 (d, 2H, $J$ = 7.70 Hz), 8.2–9.0 (broad signal, P–OH) $^{13}$C-NMR (125.7 MHz, DMSO-$d_6$) $\delta$/ppm = 127.1, 127.2, 127.5, 127.6, 129.5, 130.5, 131.7, 133.6, 134.8, 138.3, 141.7, 143.9 (aromatic C), 167.5 (–COOH). $^{31}$P-NMR (121.5 MHz, DMSO-$d_6$) $\delta$/ppm = 10.91. Spectra are given in

Fig. S9–S12 in ESI.† EI-MS(+) at 260 °C, M = C$_{13}$H$_{11}$O$_5$P, (278): $m/z$ (%) 278 (100) [M], 198 (22) [M–PO$_3$H]$^+$, 152 (40) [M–PO$_3$H$_2$–CO$_2$H = C$_{12}$H$_8$]$^+$. Calcd. for C$_{13}$H$_{11}$O$_5$P (278.2 g mol$^{-1}$): C 56.13, H 3.99%. Found C 56.17, H 4.10%.

**[Zn$_5$($\mu_3$-OH)$_4$($\mu_4$-O$_3$P–(C$_6$H$_4$)$_2$–CO$_2$-$\mu_2$)$_2$] (5).** In a Teflon-lined stainless-steel autoclave portions of 9.9 mg (0.054 mmol) of anhydrous zinc acetate (Zn(OAc)$_2$), 10.0 mg (0.036 mmol) of H$_3$BPPA and 2.4 mg (0.03 mmol) of oxalic acid dihydrate (C$_2$H$_2$O$_4$·2H$_2$O) were mixed in 1 mL of doubly deionized water and heated to 190 °C for 72 h. After cooling to ambient temperature within 24 h colorless, needle-shaped crystals were obtained. Crystal yield 17.0 mg (51%); adjustment of the reactant stoichiometry to the ratio found in the X-ray structure of the product does have little effect on the yield. The synthesis of **5** also led to the formation of plate-like, colorless crystals, which were found at the bottom of the reaction vessel. It was shown through the independent synthesis of **6** that those were crystals of **6**, which had been formed as by-product to **5** (Fig. S25 and S26 in ESI†). Mp > 300 °C. FT-IR (ATR) $\tilde{v}$/cm$^{-1}$ = 3460 (w), 3069 (w), 1691 (w), 1586 (w), 1553 (w), 1519 (w), 1423 (m), 1167 (m), 1143 (m), 1073 (vs), 962 (vs), 925 (s), 869 (m), 830 (s), 775 (vs), 728 (m), 700 (m), 595 (vs) (Fig. S13, ESI†). Calc. for C$_{26}$H$_{20}$O$_{14}$P$_2$Zn$_5$ (945.29 g mol$^{-1}$): C 33.04, H 2.13%. Found C 33.71, H 2.39%.

**[Zn($\mu_6$-O$_3$P–(C$_6$H$_4$)$_2$–CO$_2$H)] (6).** In a Teflon-lined stainless-steel autoclave 18.8 mg (0.072 mmol) of Zn(NO$_3$)$_2$·4H$_2$O and 20.0 mg (0.072 mmol) of H$_3$BPPA combined with 2 mL of DI water. The suspension was stirred briefly and then kept in a programmable oven at 200 °C for 48 h and then cooled to ambient temperature within 24 h. An off-white crystalline powder was obtained, which was washed with portions of DI water (3 × 5 mL) and dried in air. Crystal yield 13.0 mg (54%). Mp > 300 °C. FT-IR (ATR) $\tilde{v}$/cm$^{-1}$ = 2988 (w, br), 2875 (w, br), 2669 (w, b), 2543 (w, br), 1681 (m), 1606 (w), 1427 (w), 1275 (w), 1179 (m), 1146 (s), 1059 (vs), 958 (vs), 828 (m), 756 (m), 691 (w), 599 (vs), 562 (s) (Fig. S14, ESI†). Calc. for C$_{13}$H$_9$O$_5$PZn (341.56 g mol$^{-1}$): C 45.71, H 2.66%. Found C 45.69, H 2.54%.

**[Cd$_3$($\mu_6$-O$_3$P–(C$_6$H$_4$)$_2$–CO$_2$-$\mu_2$)($\mu_6$-O$_3$P–(C$_6$H$_4$)$_2$–CO$_2$-$\mu_3$)] (7).** Portions of 14.0 mg (0.053 mmol) of Cd(OAc)$_2$·2H$_2$O, 10.0 mg (0.036 mmol) of H$_3$BPPA, 3.6 mg (0.029 mmol) of oxalic acid dihydrate (C$_2$H$_2$O$_4$·2H$_2$O) and 3 mL of DI water were placed in a Teflon-lined stainless-steel autoclave, which was heated to 190 °C within six hours, kept at this temperature for 48 h and then cooled to room temperature over 24 h. The product was filtered, washed with water (3 × 10 mL) and dried in air to obtain a white powder. Yield 15.0 mg (94%). Mp > 300 °C. FT-IR (ATR) $\tilde{v}$/cm$^{-1}$ = 3402 (m, b), 3284 (m), 2855 (w, b), 2546 (w), 1684 (vs), 1604 (m), 1425 (s), 1126 (m), 1089 (s), 1031 (m), 948 (s), 823 (s), 765 (s), 719 (s), 687 (m), 578 (s) (Fig. S15, ESI†). Calc. for C$_{26}$H$_{16}$Cd$_3$O$_{10}$P$_2$ (887.59 g mol$^{-1}$): C 35.18, H 1.82%. Found C, 35.26, H 2.0%.

**[Hg($\mu_3$-HO$_3$P–(C$_6$H$_4$)$_2$–CO$_2$H)] (8).** *Caution: Elemental mercury and its compounds are highly toxic and should be handled under adequate safety conditions, wearing gloves, dust mask and using fumehoods!*

Inside a Teflon-lined stainless-steel autoclave 11.0 mg (0.034 mmol) of $Hg(OAc)_2$ and 3.6 mg (0.029 mmol) of oxalic acid dihydrate were weighed and dissolved in 4 mL of DI water. A portion of 10.0 mg (0.036 mmol) of $H_3BPPA$ was added and the suspension stirred to homogeneity. The reactor was heated to 120 °C within 24 h and kept at this temperature for 72 h. After cooling to room temperature within 24 h the solids were filtered and washed with water (3 × 10 mL). Colorless block-shaped crystals of very small size (0.01 × 0.01 × 0.01 mm) were isolated, which were used for X-ray structure determination. Crystal yield 8.0 mg (50%). Mp > 300 °C. FT-IR (ATR) $\tilde{v}/cm^{-1}$ = 2969 (m, br) 2849 (m, br), 2674 (w), 2547 (w), 2323 (w), 1807 (w), 1682 (vs), 1604 (m), 1573 (w), 1426 (m), 1392 (m), 1280 (m), 1139 (m), 1070 (m), 824 (s), 765 (s), 752 (m), 720 (m), 582 (s) (Fig. S16, ESI†). Calc. for $C_{13}H_{10}HgO_5P$ (477.78 g $mol^{-1}$): C 32.68, H 2.11%. Found C 30.84, H 1.91%.

[$Co(\mu_6-O_3P-(C_6H_4)_2-CO_2H)$] (9). In a Teflon-lined stainless-steel autoclave 9.32 mg (0.036 mmol) of anhydrous $CoCl_2$ and 10.0 mg (0.036 mmol) of $H_3BPPA$ were suspended in 2 mL DI water and heated at 220 °C for 48 h. After cooling to ambient temperature over 24 h very thin pink-colored hexagonal plate-shaped crystals were formed with dimensions of 0.01 × 0.01 × 0.001 mm. Crystal yield 16.0 mg (61%). Mp = >300 °C. FT-IR (ATR) $\tilde{v}/cm^{-1}$ = 3445 (w, b), 2961 (w, br), 2777 (w, br), 1681 (m), 1602 (w), 1419 (m), 1390 (m), 1138 (m), 944 (vs), 828 (s), 768 (s), 753 (m), 723 (m), 579 (m) (Fig. S17, ESI†). Calc. for $C_{13}H_9CoO_5P$ (335.12 g $mol^{-1}$): C 46.59, H 2.71%. Found: C 46.16, H 3.24%.

## Notes and references

1 N. Stock and S. Biswas, *Chem. Rev.*, 2012, **112**, 933–969; M. Gaab, N. Trukhan, S. Maurer, R. Gummaraju and U. Müller, *Microporous Mesoporous Mater.*, 2012, **157**, 131–136; C. Janiak and J. K. Vieth, *New J. Chem.*, 2010, **34**, 2366–2388; C. Janiak, *Dalton Trans.*, 2003, 2781–2804.

2 S. Li and F. Huo, *Nanoscale*, 2015, 7, 7482–7501.

3 A. H. Chughtai, N. Ahmad, H. A. Younus, A. Laypkovc and F. Verpoort, *Chem. Soc. Rev.*, 2015, **44**, 6804–6849.

4 Y. Xu, M. Wu, Y. Liu, X.-Z. Feng, X.-B. Yin, X.-W. He and Y.-K. Zhang, *Chem. – Eur. J.*, 2013, **19**, 2276–2283.

5 B. Gole, A. K. Bar and P. S. Mukherjee, *Chem. – Eur. J.*, 2014, **20**, 13321–13336.

6 R. B. Getman, Y.-S. Bae, C. E. Wilmer and R. Q. Snurr, *Chem. Rev.*, 2012, **112**, 703–723; L. Wu, M. Xue, S.-L. Qiu, G. Chaplais, A. Simon-Masseron and J. Patarin, *Microporous Mesoporous Mater.*, 2012, **157**, 75–81; R. J. Kuppler, D. J. Timmons, Q.-R. Fang, J.-R. Li, T. A. Makal, M. D. Young, D. Yuan, D. Zhao, W. Zhuang and H.-C. Zhou, *Coord. Chem. Rev.*, 2009, **253**, 3042–3066; M. P. Suh, H. J. Park, T. K. Prasad and D. W. Lim, *Chem. Rev.*, 2012, **112**, 782–835; H. Wu, Q. Gong, D. H. Olson and J. Li, *Chem. Rev.*, 2012, **112**, 836–868; L. J. Murray, M. Dincă and J. R. Long, *Chem. Soc. Rev.*, 2009, **38**, 1294–1314.

7 J. A. Mason, M. Veenstra and J. R. Long, *Chem. Sci.*, 2014, **5**, 32–51; R. Sathre and E. Masanet, *RSC Adv.*, 2013, **3**, 4964–4975; J. Liu, P. K. Thallapally, B. P. McGrail, D. R. Bown and J. Liu, *Chem. Soc. Rev.*, 2012, **41**, 2308–2322; H. Amrouche, B. Creton, F. Siperstein and C. Nieto-Draghi, *RSC Adv.*, 2012, **2**, 6028–6035.

8 J. R. Li, J. Sculley and H. C. Zhou, *Chem. Rev.*, 2012, **112**, 869–932; Z. Zhang, Y. Zhao, Q. Gong, Z. Li and J. Li, *Chem. Commun.*, 2013, **49**, 653–661; H. B. Tanh Jeazet, C. Staudt and C. Janiak, *Dalton Trans.*, 2012, **41**, 14003–14027; X. Y. Chen, V.-T. Hoang, D. Rodrigue and S. Kaliaguine, *RSC Adv.*, 2013, **3**, 24266–24279; G. Férey, C. Serre, T. Devic, G. Maurin, H. Jobic, P. L. Llewellyn, G. De Weireld, A. Vimont, M. Daturi and J. S. Chang, *Chem. Soc. Rev.*, 2011, **40**, 550–562; J.-R. Li, Y. Ma, M. C. McCarthy, J. Sculley, J. Yu, H.-K. Jeong, P. B. Balbuena and H.-C. Zhou, *Coord. Chem. Rev.*, 2011, **255**, 1791–1823; N. Hara, M. Yoshimune, H. Negishi, K. Haraya, S. Hara and T. Yamaguchi, *RSC Adv.*, 2013, **3**, 14233–14236; J. H. Yoon, D. Kim, X. Song, S. Han, J. Shin, S. B. Hong and M. Soo Lah, *RSC Adv.*, 2012, **2**, 11566–11573; M. Fischer, F. Hoffmann and M. Fröba, *RSC Adv.*, 2012, **2**, 4382–4396; L. Ge, A. Du. M. Hou, V. Rudolph and Z. Zhu, *RSC Adv.*, 2012, **2**, 11793–11800; Z. R. Herm, R. Krishna and J. R. Long, *Microporous Mesoporous Mater.*, 2012, **157**, 94–100; M. G. Plaza, A. F. P. Ferreira, J. C. Santos, A. M. Ribeiro, U. Müller, N. Trukhan, J. M. Loureiro and A. E. Rodrigues, *Microporous Mesoporous Mater.*, 2012, **157**, 101–111.

9 S. Qiu, M. Xue and G. Zhu, *Chem. Soc. Rev.*, 2014, **43**, 6116–6140.

10 F. Jeremias, D. Fröhlich, C. Janiak and S. Henninger, *New J. Chem.*, 2014, **4**, 24073–24082; C. Janiak and S. K. Henninger, *Chimia*, 2013, **67**, 419–424; M. Taddei, A. Ienco, F. Costantino and A. Guern, *RSC Adv.*, 2013, **3**, 26177–26183; P. Küsgens, M. Rose, I. Senkovska, H. Fröde, A. Henschel, S. Siegle and S. Kaskel, *Microporous Mesoporous Mater.*, 2009, **120**, 325–330; J. J. Low, A. I. Benin, P. Jakubczak, J. F. Abrahamian, S. A. Faheem and R. R. Willis, *J. Am. Chem. Soc.*, 2009, **131**, 15834–15842.

11 G. Férey, *Dalton Trans.*, 2009, 4400–4415; G. Férey and C. Serre, *Chem. Soc. Rev.*, 2009, **38**, 1380–1399; G. Férey, *Chem. Soc. Rev.*, 2008, **37**, 191–214.

12 G. Férey, C. Serre, C. Mellot-Draznieks, F. Millange, S. Surble, J. Dutour and I. Margiolaki, *Angew. Chem., Int. Ed.*, 2004, **43**, 6296–6301; P. Horcajada, S. Surble, C. Serre, D.-Y. Hong, Y.-K. Seo, J.-S. Chang, J.-M. Grenèche, I. Margiolaki and G. Férey, *Chem. Commun.*, 2007, 2820–2822; L. Kurfiřtová, Y.-K. Seo, Y.-K. Hwang, J.-S. Chang and J. Čejka, *Catal. Today*, 2012, **179**, 85–90.

13 G. Férey, C. Mellot-Draznieks, C. Serre, F. Millange, J. Dutour, S. Surble and I. Margiolaki, *Science*, 2005, **309**, 2040–2042.

14 G. Akiyama, R. Matsuda and S. Kitagawa, *Chem. Lett.*, 2010, **39**, 360–361.

15 M. Kandiah, M. H. Nilsen, S. Usseglio, S. Jakobsen, U. Olsbye, M. Tilset, C. Larabi, E. A. Quadrelli, F. Bonino and K. P. Lillerud, *Chem. Mater.*, 2010, **22**, 6632–6640; J. H. Cavka, S. Jakobsen, U. Olsbye, N. Guillou, C. Lamberti, S. Bordiga and K. P. Lillerud, *J. Am. Chem. Soc.*, 2008, **130**, 13850–13851.

16 N. C. Burtch, H. Jasuja and K. S. Walton, *Chem. Rev.*, 2014, **114**, 10575–10612.

17 J. Canivet, A. Fateeva, Y. Guo, B. Coasnec and D. Farrusseng, *Chem. Soc. Rev.*, 2014, **43**, 5594–5617.

18 F. Jeremias, V. Lozan, S. Henninger and C. Janiak, *Dalton Trans.*, 2013, **42**, 15967–15973; A. Khutia, H. U. Rammelberg, T. Schmidt, S. Henninger and C. Janiak, *Chem. Mater.*, 2013, **25**, 790–798; J. Ehrenmann, S. K. Henninger and C. Janiak, *Eur. J. Inorg. Chem.*, 2011, 471–474.

19 C. Heering, I. Boldog, V. Vasylyeva, J. Sanchiz and C. Janiak, *CrystEngComm*, 2013, **15**, 9757–9768.

20 C. Montoro, F. Linares, E. Quartapelle Procopio, I. Senkovska, S. Kaskel, S. Galli, N. Masciocchi, E. Barea and J. A. R. Navarro, *J. Am. Chem. Soc.*, 2011, **133**, 11888–11891.

21 P. O. Adelani, L. J. Jouffret, J. E. S. Szymanowski and P. C. Burns, *Inorg. Chem.*, 2012, **51**, 12032–12040.

22 P. O. Adelani, G. E. Sigmon and P. C. Burns, *Inorg. Chem.*, 2013, **52**, 6245–6247.

23 Reviews: K. Maeda, *Microporous Mesoporous Mater.*, 2004, **73**, 47–55; A. Clearfield and Z. Wang, *J. Chem. Soc., Dalton Trans.*, 2002, 2937–2947; A. Clearfield, *Curr. Opin. Solid State Mater. Sci.*, 2002, **6**, 495–506.

24 S. Kirumakki, J. Huang, A. Subbiah, J. Yao, A. Rowland, B. Smith, A. Mukherjee, S. Samarajeewa and A. Clearfield, *J. Mater. Chem.*, 2009, **19**, 2593–2603.

25 F. Zhai, Q. Zheng, Z. Chen, Y. Ling, X. Liu, L. Wenig and Y. Zhou, *CrystEngComm*, 2013, **15**, 2040–2043.

26 S. Kirumakki, J. Huang, A. Subbiah, J. Yao, A. Rowland, B. Smith, A. Mukherjee, S. Samarajeewa and A. Clearfield, *J. Mater. Chem.*, 2008, **19**, 2593–2603.

27 X. Zhao, J. G. Bell, S.-F. Tang, L. Li and K. M. Thomas, *J. Mater. Chem. A*, 2016, **4**, 1353–1365.

28 A. Clearfield and K. Demadis, *Metal Phosphonate Chemistry: From Synthesis to Applications*, Royal Society of Chemistry, Oxford, 2012, ch. 2–4, pp. 45–128.

29 M. Deng, X. Liu, Q. Zheng, Z. Chen, C. Fang, B. Yue and H. He, *CrystEngComm*, 2013, **15**, 7056–7061.

30 K. J. Gagnon, H. P. Perry and A. Clearfield, *Chem. Rev.*, 2012, **112**, 1034–1054.

31 J. M. Taylor, R. Vaidhyanathan, S. S. Iremonger and G. K. H. Shimizu, *J. Am. Chem. Soc.*, 2012, **134**, 14338–14340.

32 T. L. Kinnibrugh, A. A. Ayi, V. I. Bakhmutov, J. Zon and A. Clearfield, *Cryst. Growth Des.*, 2013, **13**, 2973–2981.

33 T. Zheng, J. M. Clemente-Juan, J. Ma, L. Dong, S.-S. Bao, J. Huang, A. Coronado and L.-M. Zheng, *Chem. – Eur. J.*, 2013, **19**, 16394–16402.

34 M. Taddei, F. Costantino, A. Lenco, A. Comotti, P. V. Dau and S. M. Cohen, *Chem. Commun.*, 2013, **49**, 1315–1317.

35 R. El Osta, M. Frigoli, J. Marrot, N. Guillou, H. Chevreau, R. I. Walton and F. Millange, *Chem. Commun.*, 2012, **48**, 10639–10641.

36 A. Clearfield and K. D. Demadis, *Metal Phosphonate Chemistry*, RSC Publishing, Cambridge, 2011.

37 A. R. Patterson, W. Schmitt and R. C. Evans, *J. Phys. Chem. C*, 2014, **118**, 10291–10301.

38 L. Jiménez-García, A. Kaltbeitzel, W. Pisula, J. S. Gutmann, M. Klapper and K. Müllen, *Angew. Chem., Int. Ed.*, 2009, **48**, 9951–9953.

39 A. Corma, H. García and F. X. Llabrés i Xamena, *Chem. Rev.*, 2010, **110**, 4606–4655.

40 G. K. H. Shimizu, R. Vaidhyanathan and J. M. Taylor, *Chem. Soc. Rev.*, 2009, **38**, 1430–1449.

41 Review: T. Rojo, J. L. Mesa, J. Lago, B. Bazan, J. L. Pizarro and M. I. Arriortua, *J. Mater. Chem.*, 2009, **19**, 3793–3818.

42 Cobalt compounds: (*a*) S.-Z. Hou, D.-K. Cao, X.-G. Liu, Y.-Z. Li and L.-M. Zheng, *Dalton Trans.*, 2009, 2746–2750; (*b*) Y. S. Ma, Y. Song and L.-M. Zheng, *Inorg. Chim. Acta*, 2008, **361**, 1363–1371; (*c*) Z.-C. Zhang, S. Gao and L.-M. Zheng, *Dalton Trans.*, 2007, 4681–4684; (*d*) L.-M. Zheng, S. Gao, P. Yin and X.-Q. Xin, *Inorg. Chem.*, 2004, **43**, 2151–2156; (*e*) P. Yin, S. Gao, L.-M. Zheng and X.-Q. Xin, *Chem. Mater.*, 2003, **15**, 3233–3236; (*f*) P. Yin, S. Gao, L.-M. Zheng, Z.-M. Wang and X.-Q. Xin, *Chem. Commun.*, 2003, 1076–1077; (*g*) P. Yin, X.-C. Wang, S. Gao and L.-M. Zheng, *J. Solid State Chem.*, 2005, **178**, 1049–1054.

43 Iron compounds: H. A. Habib, B. Gil-Hernández, K. Abu-Shandi, J. Sanchiz and C. Janiak, *Polyhedron*, 2010, **29**, 2537–2545; K. Abu-Shandi, H. Winkler and C. Janiak, *Z. Naturforsch. B*, 2006, **632**, 629–633; K. Abu-Shandi and C. Janiak, *Z. Naturforsch. B.*, 2005, **60**, 1250–1254; Y. Lalatonne, C. Paris, J. M. Serfaty, P. Weinmann, M. Lecouvey and L. Motte, *Chem. Commun.*, 2008, 2553–2555; C. A. Merrill and A. K. Cheetham, *Inorg. Chem.*, 2005, **44**, 5273–5277; H.-H. Song, L.-M. Zheng, G.-S. Zhu, Z. Shi, S.-H. Feng, S. Gao, Z. Hu and X.-Q. Xin, *J. Solid State Chem.*, 2002, **164**, 367–373; M. Riou-Cavellec, C. Serre, J. Robino, M. Noguès, J.-M. Grenèche and G. Férey, *J. Solid State Chem.*, 1999, **147**, 122–131; L.-M. Zheng, H.-H. Song, C.-H. Lin, S.-L. Wang, Z. Hu, Z. Yu and X.-Q. Xin, *Inorg. Chem.*, 1999, **38**, 4618–4619; A. W. Herlinger, J. R. Ferraro, J. A. Garcia and R. Chiarizia, *Polyhedron*, 1998, **17**, 1471–1475.

44 J.-S. Feng, S.-S. Bao, M. Ren, Z.-S. Cai and L.-M. Zheng, *Chem. – Eur. J.*, 2015, **21**, 17336–17343.

45 X.-J. Yang, S.-S. Bao, M. Ren, N. Hoshino, T. Akutagawa and L.-M. Zheng, *Chem. Commun.*, 2014, **50**, 3979–3981.

46 Y.-Z. Zheng and R. E. P. Winpenny, *Sci. China: Chem.*, 2012, **55**, 910–913.

47 Z.-Y. Du, H.-R. Wen, C.-M. Liu, Y.-H. Sun, Y.-B. Lu and Y.-R. Xie, *Cryst. Growth Des.*, 2010, **10**, 3721–3726.

48  Y.-Y. Zhang, M.-H. Zeng, Y. Qi, S.-Y. Sang and Z.-M. Liu, *Inorg. Chem. Commun.*, 2007, **10**, 33–36.

49  M. Menelaou, M. Dakanali, C. P. Raptopoulou, C. Drouza, N. Lalioti and A. Salifoglou, *Polyhedron*, 2009, **28**, 3331–3339; S. Kunnas-Hiltunen, M. Matilainen, J. J. Vepsäläinen and M. Ahlgrén, *Polyhedron*, 2009, **28**, 200–204; P. J. Byrne, D. S. Wragg, J. E. Warren and R. E. Morris, *Dalton Trans.*, 2009, 795–799; C.-Y. Fang, Z.-X. Chen, X.-F. Liu, Y.-T. Yang, M.-L. Deng, L.-H. Weng, Y. Jia and Y.-M. Zhou, *Inorg. Chim. Acta*, 2009, **362**, 2101–2107; K. Latham, K. F. White, K. B. Szpakolski, C. J. Rix and J. M. White, *Inorg. Chim. Acta*, 2009, **362**, 1872–1886; G. Yucesan, J. E. Valeich, H. X. Liu, W. Ouellette, C. J. O'Connor and J. Zubieta, *Inorg. Chim. Acta*, 2009, **362**, 1831–1839; J. Galezowska, P. Kafarski, H. Kozlowski, P. Mlynarz, V. M. Nurchi and T. Pivetta, *Inorg. Chim. Acta*, 2009, **362**, 707–713; Z. Y. Du, Y. R. Xie and H. R. Wen, *Inorg. Chim. Acta*, 2009, **362**, 351–354; S. M. Ying, X. F. Li, J. G. Huang, J. Y. Lin, W. T. Chen and G. P. Zhou, *Inorg. Chim. Acta*, 2008, **361**, 1547–1551; D. R. Jansen, J. R. Zeevaart, Z. I. Kolar, K. Djanashvili, J. A. Peters and G. C. Krijger, *Polyhedron*, 2008, **27**, 1779–1786; R. Murugavel and S. Shanmugan, *Dalton Trans.*, 2008, 5358–5367; V. Chandrasekhar, P. Sasikumar and R. Boomishankar, *Dalton Trans.*, 2008, 5189–5196.

50  C. Heering, B. Nateghi and C. Janiak, *Crystals*, 2016, **6**, 22.

51  J. Svoboda, V. Zima, L. Beneš, K. Melánová, M. Trchová and M. Vlček, *Solid State Sci.*, 2008, **10**, 1533–1542.

52  A.-M. Pütz, L. M. Carrella and E. Rentschler, *Dalton Trans.*, 2013, **42**, 16194–16199.

53  J.-M. Rueff, N. Barrier, S. Boudin, V. Dorcet, V. Caignaert, P. Boullay, G. B. Hix and P.-A. Jaffrès, *Dalton Trans.*, 2009, 10614–10620.

54  J.-M. Rueff, O. Perez, A. Leclaire, H. Couthon-Gourvès and P.-A. Jaffrès, *Eur. J. Inorg. Chem.*, 2009, 4870–4876.

55  J.-T. Li, L.-R. Guo, Y. Shen and L.-M. Zheng, *CrystEngComm*, 2009, **11**, 1674–1678.

56  J.-M. Rueff, O. Perez, V. Caignaert, G. Hix, M. Berchel, F. Quentel and P.-A. Jaffrès, *Inorg. Chem.*, 2015, **54**, 2152–2159.

57  V. Zima, J. Svoboda, L. Beneš, K. Melánová, M. Trchová and J. Dybal, *J. Solid State Chem.*, 2007, **180**, 929–939.

58  P. O. Adelani and T. E. Albrecht-Schmitt, *Inorg. Chem.*, 2010, **49**, 5701–5705.

59  K. Melánová, J. Klevcov, L. Beneš, J. Svoboda and V. Zima, *J. Phys. Chem. Solids*, 2012, **73**, 1452–1455.

60  J.-T. Li, D.-K. Cao, T. Akutagawa and L.-M. Zheng, *Dalton Trans.*, 2010, **39**, 8606–8608.

61  Z. Chen, Y. Zhou, L. Weng and D. Zhao, *Cryst. Growth Des.*, 2008, **8**, 4045–4053.

62  Y. Ling, M. Deng, Z. Chen, B. Xia, X. Liu, Y. Yang, Y. Zhou and L. Wenig, *Chem. Commun.*, 2013, **49**, 78–80.

63  B. A. Breeze, M. Shanmugam, F. Tuna and R. E. P. Winpenny, *Chem. Commun.*, 2007, 5185–5187.

64  J.-M. Rueff, O. Perez, A. Leclaire, H. Couthon-Gourvès and P.-A. Jaffrès, *Eur. J. Inorg. Chem.*, 2009, 4870–4876.

65  T.-B. Liao, Y. Ling, Z.-X. Chen, Y.-M. Zhou and L.-H. Weng, *Chem. Commun.*, 2010, **46**, 1100–1102.

66  E. B. Merkushev and N. D. Yudina, *Zh. Org. Khim.*, 1982, **17**, 2598–2601.

67  C. P. Brock, J. R. Blackburn and K. L. Haller, *Acta Crystallogr., Sect. B: Struct. Sci.*, 1984, **40**, 493–498.

68  H. D. Flack, M. Sadki, A. L. Thompson and D. J. Watkin, *Acta Crystallogr., Sect. A: Found. Crystallogr.*, 2011, **67**, 21–34; H. D. Flack and G. Bernardinelli, *Chirality*, 2008, **20**, 681–690; H. D. Flack and G. Bernardinelli, *Acta Crystallogr., Sect. A: Found. Crystallogr.*, 1999, **55**, 908–915; H. Flack, *Acta Crystallogr., Sect. A: Found. Crystallogr.*, 1983, **39**, 876–881; S. Parsons, H. D. Flack and T. Wagner, *Acta Crystallogr., Sect. B: Struct. Sci.*, 2009, **69**, 249–259.

69  R. B. DeVasher, L. R. Moore and K. H. Shaughnessy, *J. Org. Chem.*, 2004, **69**, 7919–7927.

70  A. W. Addison, T. N. Rao, J. Reedijk, J. van Rijn and G. C. Verschoor, *J. Chem. Soc., Dalton Trans.*, 1984, 1349–1356.

71  A.-C. Chamayou, G. Makhloufi, L. A. Nafie, C. Janiak and S. Lüdeke, *Inorg. Chem.*, 2015, **54**, 2193–2203.

72  B. Gil-Hernández, J. K. Maclaren, H. A. Höppe, J. Pasan, J. Sanchiz and C. Janiak, *CrystEngComm*, 2012, **14**, 2635–2644; B. Gil-Hernández, H. Höppe, J. K. Vieth, J. Sanchiz and C. Janiak, *Chem. Commun.*, 2010, **46**, 8270–8272.

73  M. Enamullah, A. Sharmin, M. Hasegawa, T. Hoshi, A.-C. Chamayou and C. Janiak, *Eur. J. Inorg. Chem.*, 2006, 2146–2154; C. Janiak, A.-C. Chamayou, A. K. M. R. Uddin, M. Uddin, K. S. Hagen and M. Enamullah, *Dalton Trans.*, 2009, 3698–3709.

74  W. Dan, X. Liu, M. Deng, Y. Ling, Z. Chen and Y. Zhou, *Inorg. Chem. Commun.*, 2013, **37**, 93–96.

75  Z. Chen, Y. Zhou, L. Weng, C. Yuan and D. Zhao, *Chem. – Asian J.*, 2007, **2**, 1549–1554.

76  M. C. Etter, *Acc. Chem. Res.*, 1990, **23**, 120–126; M. C. Etter, J. C. MacDonald and J. Bernstein, *Acta Crystallogr., Sect. B: Struct. Sci.*, 1990, **46**, 256–262; M. C. Etter, *J. Phys. Chem.*, 1991, **95**, 4601–4610.

77  E. I. Stiefel and G. F. Brown, *Inorg. Chem.*, 1972, **11**, 434.

78  S. Banerjee, A. Ghosh, B. Wu, P.-G. Lassahn and C. Janiak, *Polyhedron*, 2005, **24**, 593–599.

79  The three letter symbols, proposed by M. O'Keeffe, can be retrieved with examples and further information from the Reticular Chemistry Structure Resource database, http://rcsr.anu.edu.au/.

80  Bond valences ($s$) calculated from the Hg–O bond lengths ($R$) according to $s = \exp(R_0 - R)/B$ and $R_0 = 1.900$ for Hg(I)–O or $1.972$ for Hg(II)–O, $B = 0.37$; program VALENCE as implemented in PLATON.

81  I. D. Brown and R. D. Shannon, *Acta Crystallogr., Sect. A: Cryst. Phys., Diffr., Theor. Gen. Crystallogr.*, 1973, **29**, 266; I. D. Brown and K. K. Wu, *Acta Crystallogr., Sect. B: Struct. Crystallogr. Cryst. Chem.*, 1976, **32**, 1957; I. D. Brown and D. Altermatt, *Acta Crystallogr. B*, 1985, **41**, 244; N. E. Brese and M. O'Keeffe, *Acta Crystallogr., Sect. B: Struct. Sci.*, 1991, **47**, 192–197; I. D. Brown, *J. Appl. Crystallogr.*, 1996, **29**, 479; I. D. Brown, *The Chemical*

*Bond in Inorganic Chemistry: The Bond Valence Model*, Oxford University Press, Oxford, 2002.

82 R. Galassi, F. Bachechi and A. Burini, *J. Mol. Struct.*, 2006, **791**, 82–88.

83 S. T. Liddle, in *Molecular Metal–Metal Bonds: Compounds, Synthesis, Properties*, Wiley-VCH Verlag, Weinheim, Germany, 2015, ch. 12.2.1.1.

84 A. Morsali and M. Y. Masoomi, *Coord. Chem. Rev.*, 2009, **253**, 1882–1905.

85 (*a*) K. Brodersen, R. Dölling and G. Liehr, *Z. Anorg. Allg. Chem.*, 1980, **464**, 17–29; (*b*) S. Panda, H. B. Singh and R. J. Butcher, *Inorg. Chem.*, 2004, **43**, 8532–8537; (*c*) Y. Li, J.-A. Zhang, Y.-B. Wang, M. Pan and C. Y. Su, *Inorg. Chem. Commun.*, 2013, **34**, 4–7.

86 C. D. L. Saunders, N. Burford, U. Werner-Zwanziger and R. McDonald, *Inorg. Chem.*, 2008, **47**, 3693–3699.

87 C. R. Samanamu, E. N. Zamora, J.-L. Montchamp and A. F. Richards, *J. Solid State Chem.*, 2008, **181**, 1462–1471.

88 B. Kamenar, A. Hergold-Brundic and M. Bruvo, *Z. Kristallogr.*, 1988, **184**, 103.

89 T. Dorn, A.-C. Chamayou and C. Janiak, *New J. Chem.*, 2006, **30**, 156–167.

90 J. K. Maclaren, J. Sanchiz, P. Gili and C. Janiak, *New J. Chem.*, 2012, **36**, 1596–1609.

91 M. Enamullah, V. Vasylyeva and C. Janiak, *Inorg. Chim. Acta*, 2013, **408**, 109–119.

92 S. Vairam and S. Govindarajan, *Thermochim. Acta*, 2004, **414**, 263–270.

93 L. W. Collins, E. K. Gibson and W. W. Wendlandt, *Thermochim. Acta*, 1975, **11**, 177–185.

94 T. Gunnlaughson, M. Glynn, G. M. Tocci, P. E. Kruger and F. M. Pfeffer, *Coord. Chem. Rev.*, 2006, **250**, 3094–3117; Y. Cui, Y. Yue, G. Qian and B. Chen, *Chem. Rev.*, 2012, **112**, 1126–1162.

95 H. A. Habib, A. Hoffmann, H. A. Höppe, G. Steinfeld and C. Janiak, *Inorg. Chem.*, 2009, **48**, 2166–2180; H. A. Habib, A. Hoffmann, H. A. Höppe and C. Janiak, *Dalton Trans.*, 2009, 1742–1751; H. A. Habib, J. Sanchiz and C. Janiak, *Dalton Trans.*, 2008, 1734–1744.

96 Z. Hu, B. J. Deibert and J. Li, *Chem. Soc. Rev.*, 2014, **43**, 5815–5840; J. Heine and K. Müller-Buschbaum, *Chem. Soc.*

*Rev.*, 2013, **42**, 9232–9242; M. D. Allendorf, C. A. Bauer, R. K. Bhakta and R. J. T. Houk, *Chem. Soc. Rev.*, 2009, **38**, 1330–1352.

97 L. E. Kreno, K. Leong, O. K. Farha, M. Allendorf, R. P. Van Duyne and J. T. Hupp, *Chem. Rev.*, 2012, **112**, 1105–1125.

98 J. W. Bridges, P. J. Creaven and R. T. Williams, *Biochem. J.*, 1965, **96**, 872–878.

99 Q. Gong, Z. Hu, B. J. Deibert, T. J. Emge, S. J. Teat, D. Banerjee, B. Mussman, N. D. Rudd and J. Li, *J. Am. Chem. Soc.*, 2014, **136**, 16724–16727.

100 A. Majumder, G. M. Rosair, A. Mallick, N. Chattopadhyay and S. Mitra, *Polyhedron*, 2006, **25**, 1753–1762.

101 (*a*) W. W. Lestari, P. Lonnecke, M. B. Sarosi, H. C. Streit, M. Adlung, C. Wickleder, M. Handke, W.-D. Einicke, R. Glaser and E. Hey-Hawkins, *CrystEngComm*, 2013, **15**, 3874–3884; (*b*) W. W. Lestari, H. C. Streit, P. Lönnecke, C. Wickleder and E. Hey-Hawkins, *Dalton Trans.*, 2014, **43**, 8188–8195.

102 APEXII, *Data collection program for the APEXII CCD area-detector system*, Bruker Analytical X-ray Systems, Madison, Wisconsin, USA, 2010.

103 SMART, Data Collection Program for the CCD Area-Detector System, *SAINT: Data Reduction and Frame Integration Program for the CCD Area-Detector System*, Bruker Analytical X-ray Systems, Madison, Wisconsin, USA, 1997.

104 G.-M. Sheldrick, *Program SADABS: Area-detector absorption correction*, University of Göttingen, Germany, 1996.

105 C. B. Hübschle, G. M. Sheldrick and B. Dittrich, *J. Appl. Crystallogr.*, 2011, **44**, 1281–1284.

106 J. Newman, *Acta Crystallogr., Sect. D: Biol. Crystallogr.*, 2006, **62**, 27–31.

107 K. Brandenburg, *DIAMOND (Version 3.2)*, Crystal and Molecular Structure Visualization, Crystal Impact – K. Brandenburg & H. Putz, Gbr: Bonn, Germany, 2009.

108 A. Spek, *Acta Crystallogr., Sect. D: Biol. Crystallogr.*, 2009, **65**, 148–155; A. L. Spek, *PLATON – A multipurpose crystallographic tool*, Utrecht University, Utrecht, The Netherlands, 2005.

109 H. O. Wirth, W. Kern and E. Schmitz, *Makromol. Chem.*, 1963, **68**(1), 66–69.

110 R. Pummerer and L. Seligsberger, *Ber. Dtsch. Chem. Ges.*, 1931, **64**, 2477–2486.